

# Straight from the source's mouth: Controls on field-constrained sediment export across the entire active Corinth Rift, central Greece

Stephen E. Watkins<sup>1,2,3</sup>  | Alexander C. Whittaker<sup>1</sup>  | Rebecca E. Bell<sup>1</sup>  |  
Sam A. S. Brooke<sup>4</sup> | Vamsi Ganti<sup>4,5</sup> | Robert L. Gawthorpe<sup>3</sup>  | Lisa C. McNeill<sup>6</sup>  |  
Casey W. Nixon<sup>3</sup>

<sup>1</sup>Department of Earth Science and Engineering, Imperial College London, London, UK

<sup>2</sup>Département des Sciences de la Terre, Université de Genève, Genève, Switzerland

<sup>3</sup>Department of Earth Science, University of Bergen, Bergen, Norway

<sup>4</sup>Department of Geography, University of California Santa Barbara, Santa Barbara, CA, USA

<sup>5</sup>Department of Earth Science, University of California Santa Barbara, Santa Barbara, CA, USA

<sup>6</sup>School of Ocean and Earth Science, National Oceanography Centre Southampton, University of Southampton, Southampton, UK

## Correspondence

Stephen E. Watkins, Département des Sciences de la Terre, Université de Genève, Genève, Switzerland.  
Email: stephen.watkins@unige.ch

## Funding information

Imperial College Janet Watson; Natural Environment Research Council (NERC) Science and Solutions; Royal Society, Grant/Award Number: RG 140109; Swiss National Fund, Grant/Award Number: N°200020\_182017; VISTA Scholarship

## Abstract

The volume and grain-size of sediment supplied from catchments fundamentally control basin stratigraphy. Despite their importance, few studies have constrained sediment budgets and grain-size exported into an active rift at the basin scale. Here, we used the Corinth Rift as a natural laboratory to quantify the controls on sediment export within an active rift. In the field, we measured the hydraulic geometries, surface grain-sizes of channel bars and full-weighted grain-size distributions of river sediment at the mouths of 47 catchments draining the rift (constituting 83% of the areal extent). Results show that the sediment grain-size increases westward along the southern coast of the Gulf of Corinth, with the coarse-fraction grain-sizes (84<sup>th</sup> percentile of weighted grain-size distribution) ranging from approximately 19 to 91 mm. We find that the median and coarse-fraction of the sieved grain-size distribution are primarily controlled by bedrock lithology, with late Quaternary uplift rates exerting a secondary control. Our results indicate that grain-size export is primarily controlled by the input grain-size within the catchment and subsequent abrasion during fluvial transport, both quantities that are sensitive to catchment lithology. We also demonstrate that the median and coarse-fraction of the grain-size distribution are predominantly transported in bedload; however, typical sand-grade particles are transported as suspended load at bankfull conditions, suggesting disparate source-to-sink transit timescales for sand and gravel. Finally, we derive both a full Holocene sediment budget and a grain-size-specific bedload discharged into the Gulf of Corinth using the grain-size measurements and previously published estimates of sediment fluxes and volumes. Results show that the bedload sediment budget is primarily comprised (~79%) of pebble to cobble grade (0.475–16 cm). Our results suggest that the grain-size of sediment export at the rift scale is particularly sensitive to catchment lithology

The peer review history for this article is available at <https://publons.com/publon/10.1111/bre.12444>

This is an open access article under the terms of the Creative Commons Attribution License, which permits use, distribution and reproduction in any medium, provided the original work is properly cited.

© 2020 The Authors. *Basin Research* published by International Association of Sedimentologists and European Association of Geoscientists and Engineers and John Wiley & Sons Ltd.

and fluvial morphodynamics, which complicates our ability to make direct inferences of tectonic and palaeoenvironmental forcing from local stratigraphic characteristics.

#### KEYWORDS

Corinth Rift, grain-size, sediment transport, bedload, sediment export, sediment budget

## 1 | INTRODUCTION

Basin stratigraphic architecture is fundamentally determined by the magnitude of sediment supply (Allen & Densmore, 2000; Armitage, Duller, Whittaker, & Allen, 2011; Cowie et al., 2006; Densmore, Allen, & Simpson, 2007; Forzoni, Storms, Whittaker, & Jager, 2014; Leeder, Harris, & Kirkby, 1998; Pechlivanidou et al., 2018), and the grain-size distribution within that supply (Allen et al., 2015; Armitage et al., 2011; Brooke, Whittaker, Armitage, D'Arcy, & Watkins, 2018; Hampson, Duller, Petter, Robinson, & Allen, 2014). In particular, well-constrained measures of grain-size in fluvial systems can be used to reconstruct palaeoslopes (Cassel & Graham, 2011; Duller et al., 2012; Garefalakis & Schlunegger, 2018; Paola & Mohrig, 1996), estimate tectonic subsidence rates through downstream fining (Michael, Whittaker, Carter, & Allen, 2014; Parsons, Michael, Whittaker, Duller, & Allen, 2012) and infer drier or wetter periods through time (Brooke et al., 2018; D'Arcy, Roda-Boluda, & Whittaker, 2017). Grain-size also plays a fundamental role in determining the spatiotemporal scales over which internal dynamics of sedimentary systems operate (Ganti, Lamb, & McElroy, 2014) and dictates sediment facies partitioning within subsiding depocentres (Allen et al., 2013; Armitage et al., 2011, 2015). Consequently, understanding the mechanics of sediment routing systems hinges on quantifying how sediment grain-size supplied by the source catchments to basins vary in space, and with respect to sediment discharges.

The interface between the source and the sink is an important place to consider the grain-size distribution and sediment discharge exported from catchments to the depositional sink (Allen, 2008). Multiple studies have shown how climate, tectonics and lithology control the sediment flux and grain-size distribution released from individual catchments that supply depocentres (Allen et al., 2015; Attal & Lavé, 2009; D'Arcy et al., 2017; Glaus et al., 2019; Litty & Schlunegger, 2017; Michael et al., 2014; Roda-Boluda, D'Arcy, McDonald, & Whittaker, 2018; Whittaker, Attal, & Allen, 2010); however, detangling the relative importance of these boundary conditions on the nature of sediment exported to depocentres has remained elusive, in part due to the role that internal sedimentary dynamics play in transforming the source signal into stratigraphy (Ganti et al., 2014; Jerolmack & Paola, 2010; Romans, Castelltort, Covault, Fildani, & Walsh, 2016).

#### Highlights

- Constrained the full weighted grain-size export for 47 rivers draining the Corinth Rift.
- Found a strong spatial grain-size export trend, with sizes increasing to the West.
- Found that grain-size distributions are primarily a result of the bedrock lithology being eroded.
- Shown that our sieved distributions are predominantly transported as bedload.
- Constrained a full-weighted grain-size specific sediment budget for the entire Corinth Rift.
- Provided a mechanistic explanation for the facies distribution observed in the Gulf.

Previous studies suggest that in some modern systems such as the Sperchios graben, central Greece, and the Apennines, Italy, active faulting exerts a first order control on the grain-size released from catchments to basins, where coarse sediment supply has been correlated with uplift in the footwall of active normal faults that cause increased slope failure within a knickzone (Pechlivanidou et al., 2018; Roda-Boluda et al., 2018; Whittaker et al., 2010). Moreover, the coarse-fraction of grain-size distributions can be preferentially stored within the sediment routing system before export, particularly in settings with high subsidence rates, indicating that sediment exported from these catchments can be significantly finer than that initially produced and transported within these catchments (Armitage et al., 2011; Ferguson, Hoey, Wathen, & Werritty, 1996; Parsons et al., 2012; Pechlivanidou et al., 2018). Several models have provided insight into the magnitude of sediment fluxes exported from tectonically active catchments to basins, and its variation over time (Cowie et al., 2006; Sinclair, Gibson, Naylor, & Morris, 2005). However, many do not incorporate the controls on grain-size from field or theoretical perspectives (cf. Allen et al., 2013; Cowie et al., 2006; Leeder et al., 1998; Watkins et al., 2018).

In contrast to the aforementioned studies, which generally focused on tectonic boundary conditions, correlations between grain-size exported from catchments and geomorphic and hydrologic variables (e.g., mean annual stream flows and historical storm intensity) have also

been established (e.g., Brooke et al., 2018; D'Arcy et al., 2017; Litty, Schlunegger, & Viveen, 2017). Multiple studies demonstrated that grain size exported from catchments with similar climate and tectonic characteristics can vary due to differences in catchment lithology (e.g., Allen et al., 2015; Rădoane, Rădoane, Dumitriu, & Miclăuș, 2008; Roda-Boluda et al., 2018). Stronger bedrock lithologies are likely to produce coarser sediment (Roda-Boluda et al., 2018), when compared with weaker bedrock, and the frequency of landslides also appears to be controlled by the relative abundance of weak and hard substrate within a catchment (Damm, Becht, Varga, & Heckmann, 2010; Guzzetti, Cardinali, & Reichenbach, 1996; Margielewski, 2006). Lithology also controls the initial grain-size into which rocks fragment (Allen et al., 2015), which is then reworked by the fluvial system. Furthermore, clast attrition rates are dependent on their constituent lithology (Attal & Lavé, 2009; Litty & Schlunegger, 2017) and abrasion can have major implications on the size of sediment exported from catchments (Dingle, Attal, & Sinclair, 2017).

While existing work has highlighted numerous contrasting controls on grain-size released from catchments in different settings, many of these studies focused on a limited number of catchments at a local scale. Consequently, we still lack a holistic understanding of the primary controls on grain-size export across multiple catchments supplying sediment to a subsiding depocentre at a regional scale. In this study, we address this knowledge gap by investigating how the grain-size and volumetric sediment budget exported from catchments varies in space at the scale of an entire rift system, the Corinth Rift, central Greece. We selected this location because the locus of sediment input and magnitudes of sediment discharge have been well constrained for the last 12 kyrs (Watkins et al., 2018), and tectonic, climatic and lithological boundary conditions are well documented in this region (Bell et al., 2009; Ford, Hemelsdaël, Mancini, & Palyvos, 2016; Ford et al., 2013; Gawthorpe et al., 2018; Nixon et al., 2016; Watkins et al., 2018).

Here, we present field measurements of the grain-size distributions exported by 47 rivers that drain 83% of the Corinth Rift by area. We use this comprehensive rift-scale grain-size dataset to: (a) investigate the geomorphic, hydraulic, lithologic and tectonic controls on grain-size export; (b) quantify the mode of sediment transport for different grain-sizes in the study rivers using sediment transport theory and hydraulic geometry measurements, and (c) couple the estimated sediment fluxes from Watkins et al. (2018) with our grain-size measurements to derive the first constrained grain-size sediment budget for an entire rift where sediment discharge and grain-sizes are explicitly coupled. Watkins et al. (2018) modelled the sediment discharge rates in the Holocene and showed that their estimates matched the seismically derived sediment accumulation rates in the underfilled basin of the

Corinth Rift; however, they did not investigate the controls on grain-size export or produce a grain-size-related sediment budget for the rift system. We begin with a summary of the geologic setting of our study area, and previous work pertaining to the study area.

## 2 | GEOLOGICAL SETTING AND PREVIOUS WORK

The Corinth Rift, central Greece, is one of the fastest extending rifts in the world with modern GPS extension rates varying from ~5 mm/year in the East to ~15 mm/year in the West (Avallone et al., 2004; Briole et al., 2000; Clarke et al., 1998; McClusky et al., 2000). The Corinth Rift initiated at ~5 Ma (Ori, 1989), and the present-day Corinth Rift geometry has been estimated to have been in place for the last ~400–800 kyr (Ford et al., 2016).

The water-filled basin associated with the active rift is known as the Gulf of Corinth, which is ~120 km long (E-W) and ~30 km at its widest (N-S; Figure 1). The Alkyonides Gulf, in the furthest northeast of the Gulf of Corinth (Figure 1) is a constituent part, but is semi-closed from the main basin. The presence of the Rion-Antirion Sill at 60 m depth at the basin's western end (Perissoratis, Piper, & Lykousis, 2000) implies that the basin is isolated during lowstands and effectively closed during highstands with respect to sediment export from the rift (Perissoratis et al., 2000). The modern depositional facies of the Gulf comprise highstand Gilbert deltas that fringe large parts of the Gulf, particularly in the south-central and eastern portion of the Gulf, and offshore drilling has revealed that the Holocene deposits in the main basin are predominantly mud/silt-grade sediments (McNeill et al., 2019; Moretti et al., 2004).

Many detailed studies have characterized the South Gulf of Corinth coastal margin (Bornovas & Rondogianni-Tsiambaou, 1983; Ford et al., 2016; Gawthorpe et al., 2018). The onshore Corinth syn-rift stratigraphy has previously been divided into a Lower, Middle and Upper Group; however, Lower and Middle groups contain broadly similar lithofacies (Backert, Ford, & Malartre, 2010; Ford et al., 2016; Ford, Williams, Malartre, Popescu, & Nichols, 2007; Rohais, Eschard, Ford, Guillocheau, & Moretti, 2007). We synthesized this stratigraphy into three main units based on lithology rather than relative age in order to investigate the role of lithology on grain-size (Figure 2). These are (i) Hellenide Basement, comprising carbonates and flysch; (ii) Syn-rift Lithology 1: uplifted Gilbert deltas and conglomerates which comprise the onshore and more proximal facies of the early Corinth Rift; (iii) Syn-rift Lithology 2: the distal portion of the early Corinth Rift syn-rift sediments deposited within a lacustrine environment (comprising finer grained lithologies, such as sandstones, siltstones, mudstones).

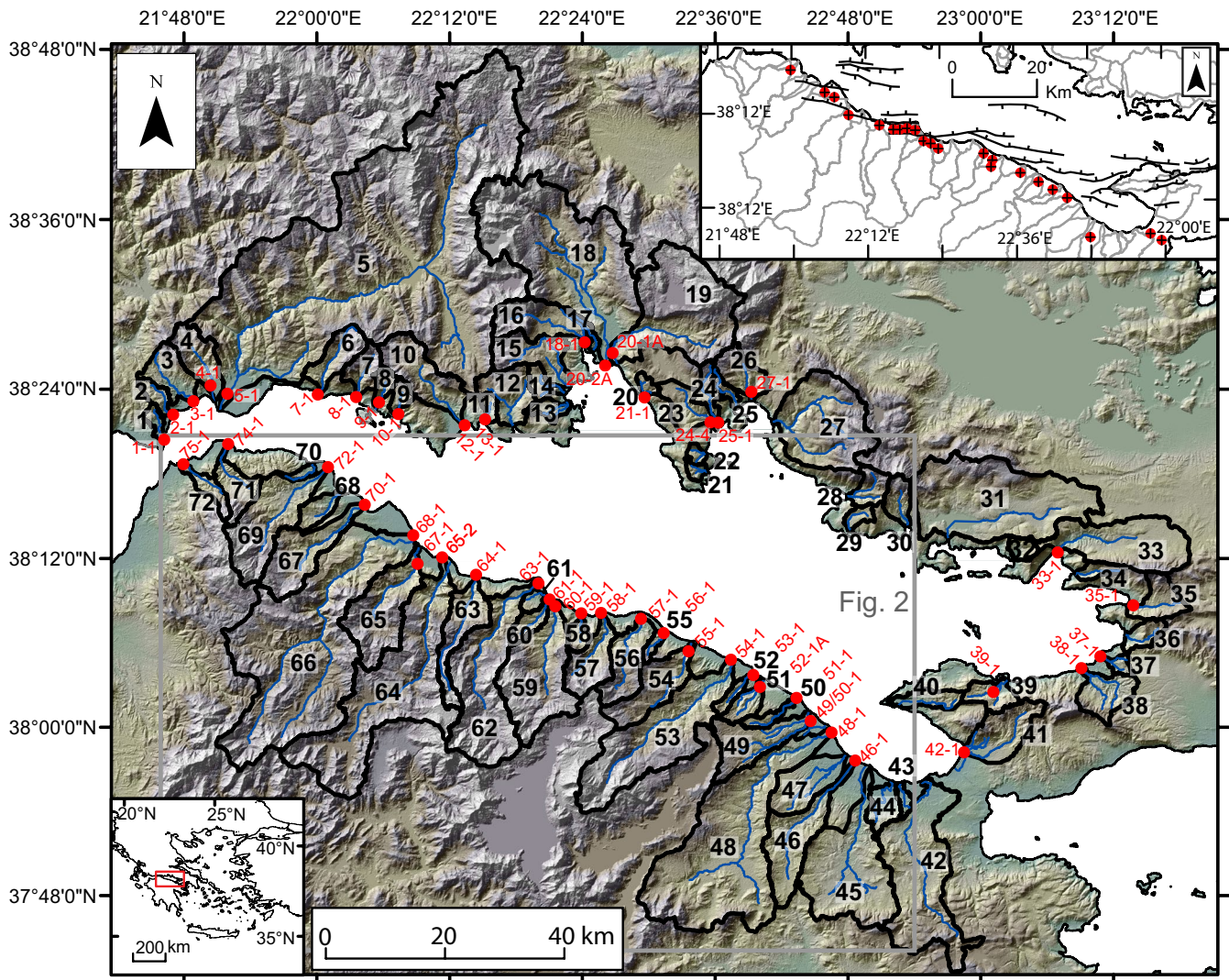


**FIGURE 1** Study area, the Corinth Rift, central Greece. Onshore topography generated using a 30 m ASTER Digital Elevation Model (DEM). Drainage network and catchments derived using ArcMap 10.1, catchments are numbered relating to the rest of the study. Red circles denote localities from the field campaign. Location of Figure 2 is outlined in a grey box. Top inset shows the location of late Quaternary uplift rates compiled by Pechlivanidou et al. (2019). Faults are from Nixon et al. (2016). Bottom inset shows the location of the Corinth Rift with respect to Greece

Previous studies have also estimated Holocene surface-uplift rates of 0.8–2 and 1.3–2.2 mm/year along the southern coastline in the footwalls of the East Eliki Fault and Derveni Fault respectively (McNeill & Collier, 2004; Mouyaris, Papastamatiou, & Vita-Finzi, 1992; Pirazzoli et al., 1994; Stewart, 1996; Stewart & Vita-Finzi, 1996). Late Quaternary surface-uplift rates derived from uplifted terraces and dated corals cover much of the South coast (compiled by Pechlivanidou et al. (2019); Figure 1-inset), and vary from 0.7–0.8 mm/year (Pspathopyrgos Fault) in the West to 0.9–1.3 mm/year for the central and eastern faults along the South coast of the Gulf of Corinth (Armijo, Meyer, King, Rigo, & Papanastassiou, 1996; De Martini et al., 2004; Houghton, Roberts, Papanikolaou, McArthur, & Gilmour, 2003; Keraudren & Sorel, 1987; McNeill & Collier, 2004; McNeill, Collier, Martini, Pantosti, & D’Addezio, 2005; McNeill et al., 2007). The North coast, however, is interpreted

to be predominantly subsiding or stable based on the sinuous coastline (Stefatos, Papatheodorou, Ferentinos, Leeder, & Collier, 2002) and subsidence markers (Bell et al., 2009).

In addition, Watkins et al. (2018) calculated suspended sediment fluxes entering the Gulf. They found that Holocene-averaged basin sediment accumulation rates (derived from a seismic reflection dataset supported by piston-core data) were directly comparable (within a factor of 1.6) to suspended sediment fluxes estimated for source catchments around the Gulf, derived using the BQART model (Syvitski & Milliman, 2007). Figure 3 shows the suspended sediment fluxes of Watkins et al. (2018) scaled to match the known sediment accumulation rates in the basin. Suspended sediment fluxes are spatially variable around the Gulf (Figure 3), with larger catchments producing higher amounts of suspended sediment. Additionally, there is a concentration of



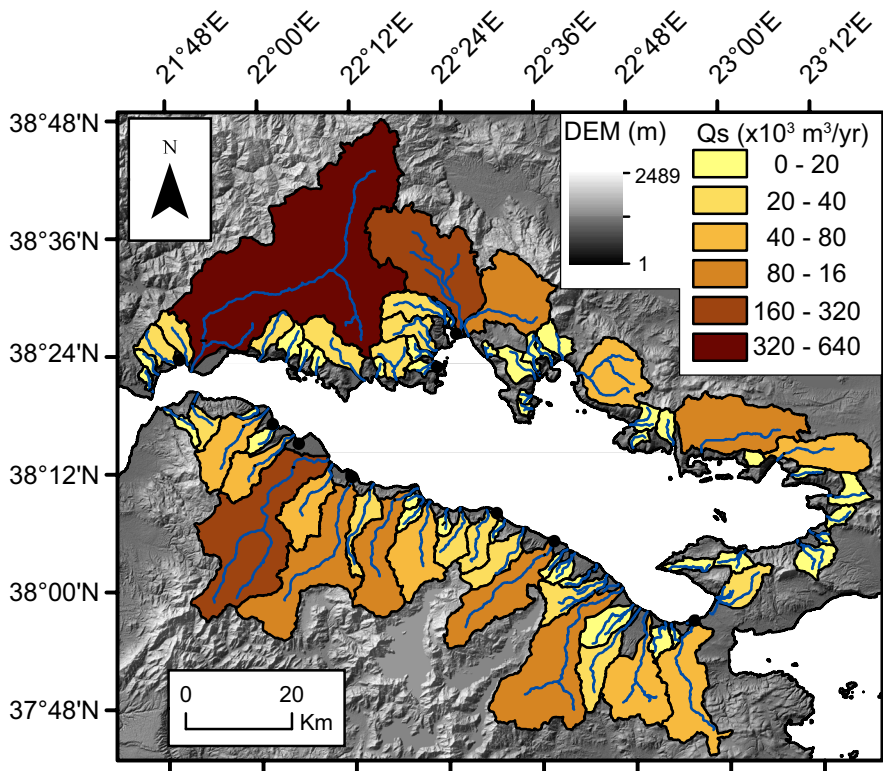


**FIGURE 3** BQART modelled annual suspended sediment fluxes from Watkins et al. (2018), scaled by 1.6 to match the Holocene basin volume ( $35 \text{ km}^3$ ), to derive the full suspended sediment flux for each catchment

- (iv) Bankfull depth,  $H_b$  (m);
- (v) Reach slope,  $S$  (degrees);

We selected high-flow channel bars for constraining the full-weighted grain-size distribution by in situ sieving, because this is the material that would be mobilized and transported at bankfull conditions (sec. Attal et al., 2015; Dingle et al., 2017; Leopold & Wolman, 1957; Whittaker et al., 2010). We removed the top layer (in order to account for armouring effects) and dug a pit into the channel bar to measure sediment size as a function of mass fraction: this method constrains the full distribution of grain-sizes exported as it temporally averages the channel bar sediment. The amount of sediment required to be sieved was dictated by the largest clast exhumed; following previous work we ensured that the largest clast was <10% by weight of the total amount sieved (cf. Kellerhals & Bray, 1971; Whittaker et al., 2010). This method ensured that the 84<sup>th</sup> percentile of the grain-size distribution ( $D_{84}$ ), a standard indicator of the coarse fraction grain-size, was captured. We sieved ~29 to 205 kg of sediment at each locality and processed a total of ~3 tonnes of sediment across our study sites. At each locality the sediment was sieved into grain-size categories of <1, 1–2, 2–4 and 4–8 cm. Clasts greater than 8 cm were weighed individually and converted to a grain-size by assuming that the clast was spherical with a density of  $2,450 \text{ kgm}^{-3}$  and then appropriately categorized into either 8–16 or 16–32 cm bins. If the largest clast was not easily recognizable (i.e. it was within the <8 cm category), we ensured that the total weight of the

largest bin size was under 10% of the total weight sieved. In one instance (catchment 24), a site had a clast with a mass of 10.8% of the total sediment measured. However, 90% of all the localities had largest clasts that were <6% of their respective total sieved weights. In order to get a finer resolution of grain-size distributions within the <1 cm fraction, we sieved a representative sample of this fraction with finer sieves. The proportions of these finer grain-size fractions were then scaled to repopulate the full-weighted grain-size distribution, given the total mass of sediment within the <1 cm fraction. The laboratory grain-size categories were 0–0.015 cm (0–150 microns), 0.015–0.025 cm (150–250 microns), 0.025–0.05 cm (250–500 microns), 0.05–0.085 cm (500–850 microns), 0.085–0.1 cm (850–1000 microns), 0.1–0.17, 0.17–0.236, 0.236–0.475 and 0.475–1 cm. At the river mouths where the channel bars had a full grain-size distribution that was finer than our 1 cm field sieve, we collected a representative sample that was later sieved in the laboratory.

We also characterized the grain-size distribution (>1 mm) of the same channel bar surface by adopting the Wolman point count method (Wolman, 1954); however, we modified this method to measure the long axis (the  $a$  axis) of 100 clasts as opposed to the intermediate axis (the  $b$  axis). We adopted this methodology because the intermediate axis can be difficult (and time consuming) to measure objectively, particularly for smaller clasts (cf. Brooke et al., 2018). Litty and Schlunegger (2017) showed that the ratio of the long and intermediate axes is relatively constant and therefore supporting measurement of the long axis only. Grain-size measurements from this

independent method were compared with the weighted grain-size distribution. In particular, we compared the  $D_{50}$  and  $D_{84}$  estimates of the Wolman point counts with the results of the sieving to test whether  $D_{50}$  and  $D_{84}$  derived from the Wolman Point count of the channel bar surface effectively captures the  $D_{50}$  and  $D_{84}$  of the subsurface data through sieving. In situ sieving captures the full-weighted grain-size distribution (including fines <1 mm) and the Wolman point count only captures the grain-size distribution of clasts greater than 1 mm of the channel bar surface. We therefore excluded the fines less than 1 mm in the in situ sieving data to compare with the point count data.

To characterize the spread of the measured grain-sizes, we show the values of  $D_{45}$ – $D_{55}$  and  $D_{79}$ – $D_{89}$  ( $D_x$  denotes the  $x^{\text{th}}$  percentile of the grain-size distribution) as grain-size bounds for the data measured using in situ sieving. The Wolman grain-size error bars were generated by comparing  $D_{50}$  at sites where multiple Wolman point counts were carried out, and we calculated the percentage difference between these independent trials. All percentage differences in median grain-size were then collated into one dataset and averaged to derive a typical error of  $\pm 15\%$  for the  $D_{50}$  from Wolman point counts.

Finally, we measured the bankfull width and depth of the channel using a laser range finder with a precision of  $\pm 4$  cm. Channel slopes were recorded (also using a laser range finder) with a precision of  $\pm 0.1^\circ$ . Maximum stage height was identified from debris (such as rafted wood, or human debris such as plastic) that showed clear indication of entrainment during high flows, or from other markers such as bleaching horizons, and lack of vegetation (Whittaker, Cowie, Attal, Tucker, & Roberts, 2007).

### 3.2 | DEM methods and constraining tectono-lithological controls on grain-size

A drainage network for the Corinth Rift was established using a 30 m spatial resolution ASTER Digital Elevation Model (DEM). We derived a stream network using the ArcGIS 10.1 hydrological toolbar, setting a threshold of 300 pixels ( $0.27 \text{ km}^2$ ). Small catchments with areas  $< 5 \text{ km}^2$  were precluded as many had no field expression or were not governed by fluvial processes. Overall 72 fluvial catchments were identified that drain into the Gulf and are numbered for identification (Figure 1).

We analysed the dependence of the measured in situ-sieved median grain-size ( $D_{50}$ ) and  $D_{84}$  on the following geomorphic and hydrologic quantities: (a) catchment drainage area,  $A$ ; (b) maximum catchment relief,  $R$ ; (c) the percentage area within a catchment with slopes  $> 30^\circ$  and; (d) mean catchment annual precipitation,  $MAP$  (m/year). These quantities were derived from the DEM and the WorldClim precipitation raster (Hijmans, Cameron, Parra, Jones, & Jarvis, 2005). We

selected these broad geomorphic and hydrologic parameters as potential variables for the following reasons: (a) Catchment area determines the length of the trunk channel, which exerts a primary control on both abrasion and selective transport of finer material downstream (c.f. Attal & Lavé, 2009). (b) Maximum catchment relief is often used as a proxy for tectonic uplift (Syvitski & Milliman, 2007), and sediment production is potentially higher in steeper, high elevation areas that may supply coarser material into the fluvial system. (c) Percentage area within a catchment of slopes  $> 30^\circ$  parameterizes the importance of landsliding, which can supply coarse material into the rivers (c.f. Litty & Schlunegger, 2017; Roda-Boluda et al., 2018; Whittaker et al., 2010). (d) Annual precipitation can control the grain-size output because high precipitation rates increase water discharge and the capacity of rivers to transport coarse sediment supplied from the hillslopes (c.f. Ferguson, Prestegard, & Ashworth, 1989; Komar & Shih, 1992). We fit a linear relationship with all parameters in the first instance, and calculate the coefficient of determination ( $r^2$ ) to evaluate the proportion of the variance in grain-size that can be attributed to these geomorphic/hydraulic variables. Additionally, we tested the null hypothesis that the linear regression coefficient is zero in the population using a two-tailed  $t$  test at a 95% significance level. This study does not consider multi-parameter dependencies.

We also evaluated the role of lithology and tectonics in controlling the eventual grain-size exported from catchments along the southern margin of the Gulf of Corinth. We used a simplified lithology map to calculate the relative percentage of different lithological groups within a given catchment (Figure 2). We also used the available late Quaternary uplift rates along the southern coast of the Gulf of Corinth (Figure 1 inset) to test if these rates correlate with the grain-size exported to the rift. We extrapolated the available late Quaternary uplift rates to obtain a trend line of uplift for the South coast, which was then applied to specific sites in our study area. These uplift rates are an indicator of net tectonic uplift over a maximum of  $\sim 400$  kyrs. This trend is different to the short-term GPS extension rates, which suggest extension rates increase strongly from East to West (e.g., Briole et al., 2000; Clarke et al., 1997; Le Pichon, Chamot-Rooke, Lallemand, Noomen, & Veis, 1995; McClusky et al., 2000; Roberts & Jackson, 1991). Our rationale, however, for comparing the measured grain-size distributions with geologically derived uplift rates, rather than geodetically measured uplift rates that average over decadal and centennial timescales, stems from previous studies that established that grain-size trends within catchments respond transiently to uplift rates over long timescales ( $\sim 800$  kyr; Roda-Boluda et al., 2018; Whittaker et al., 2010; Whittaker et al., 2007). In this study we present our field data and investigate the correlation between individual parameters and the grain size distributions measured; we do not quantify the interactions and dependencies between numerous parameters controlling grain size using multivariate approaches.

### 3.3 | Hydraulic controls on sediment export

The mode of sediment transport that dominates export of sediment is important because it dictates the nature of the sediment that fills the basin, and determines the transit time of sediment through the catchment. Over long timescales, the frequency-magnitude trade-offs of sediment transport indicate that sediment discharge is maximized for the bankfull flows (Wolman & Miller, 1960). We quantified the primary mode of sediment transport (i.e. bedload, mixed-load or suspended-load) within each catchment draining into the Gulf using the measurements of  $D_{50}$  and  $D_{84}$ , and the bankfull characteristics of the channel. Turbulent velocity fluctuations, which scale with the shear velocity ( $u_*$ ) of the flow, determine the potential for a sediment particle to be entrained into the flow. This vertical force is balanced by gravitational force parameterized by the sediment settling velocity,  $W_s$ . The ratio of these velocities,  $W_s/u_*$ , is important to constrain (e.g., Bagnold, 1966), and was specifically used by Dade and Friend (1998) to determine the dominant mode of sediment transport: for example  $W_s/u_* \geq 3$  corresponded to bedload-dominated sediment transport regime,  $W_s/u_* \leq 0.3$  corresponded to suspension-dominated sediment transport regime and  $0.3 \leq W_s/u_* \leq 3$  corresponded to the mixed-load sediment transport regime where sediment transport occurs through bedload and intermittent suspension.

We estimated the settling velocity of  $D_{50}$  and  $D_{84}$  sediment sizes and for a typical sand-grade particle (0.25 mm) using the method of Ferguson and Church (2004), see Appendix A. Shear velocity is related to the bed shear stress,  $\tau_b$ , by (e.g., Dade & Friend, 1998):

$$u_* = \sqrt{\frac{\tau_b}{\rho_w}}, \quad (1)$$

where  $\rho_w$  is density of water. We estimated the bed shear stress under bankfull conditions by assuming steady and uniform flow conditions, where the bed shear stress was approximated as the depth slope product, that is  $\tau_b = \rho_w g R_H S$ , where  $g$  is gravity,  $R_H$  is hydraulic radius and  $S$  is slope (Appendix A). The shear stress approximation used here is only valid upstream of the backwater reach—a portion of the river where non-uniform flow dominates due to the upstream influence of the receiving basin (e.g., Lamb, Nittrouer, Mohrig, & Shaw, 2012). Rivers with steep slopes and shallow flow depths are expected to have a short backwater reach (Paola & Mohrig, 1996), and we excluded the localities where data were collected within a distance less than the estimated backwater length upstream of the river mouth (see Appendix A).

### 3.4 | Estimating the total Holocene sediment budget for the rift

We estimated a total Holocene sediment budget for the Corinth Rift building on the previous work of Watkins et al.

(2018). Using seismic reflection data, Watkins et al. (2018) determined that the volume of Holocene-aged sediment within the Corinth basin (the Gulf of Corinth) is  $35 \text{ km}^3$ . This is likely the suspended fraction of the budget as long-piston cores (Moretti et al., 2004) and IODP drilling results (McNeill et al., 2019) suggest that Holocene sediment is predominantly silts and sands. To quantify the total Holocene sediment budget averaged over the Holocene, we estimated the bedload sediment budget using a range of ratios. This is because the ratio of bedload to suspended load has been shown to be highly variable and also difficult to obtain (e.g., Turowski, Rickenmann, & Dadson, 2010), as such we adopt the ratio of 35:65 bedload to suspended load (Pratt-Sitaula et al., 2007) with upper and lower ratios of 45:55 and 25:75, respectively, based off field data, to acknowledge the wide uncertainties. We adopted a ratio of 35:65 for bedload to suspended load (Pratt-Sitaula et al., 2007), which is based on field-derived bedload and suspended fractions from the Marsyandi River, Himalayas, a steep gravel-bedded mountain catchment for the last 5,000 years (Pratt-Sitaula et al., 2007). We also acknowledge that the ratio of bedload to total sediment flux can vary from <25% to >50% in the natural settings (e.g., Turowski et al., 2010). To better characterize this range of variability in bedload to suspended load ratios, we also computed the total Holocene sediment budget using bedload to suspended sediment load ratios of 25:75 and 45:55, values consistent with the modern field observations of Turowski et al. (2010) in the Pitzbach catchment, Austria.

Finally, we investigate the median grain-size around the Gulf that is at the threshold of suspension ( $W_s/u_* = 0.3$ ). This estimated grain-size (0.085 cm, results below) defines the grain-sizes that the bulk suspended sediment volume (i.e. 0–0.085 cm) and bulk bedload sediment volume (0.085–32 cm) represent.

### 3.5 | Deriving the grain-size-specific bedload discharge for the Holocene

To estimate a grain-size-specific bedload discharge for the Holocene, we require sediment flux data for each sieved river. Watkins et al. (2018) derived annual suspended sediment fluxes using the BQART method for every river draining into the Gulf. When these fluxes were summed and scaled over the Holocene (i.e. summed over 12,000 years), a suspended volume of  $21.3 \text{ km}^3$  was obtained for the period, which was similar in magnitude to the known Holocene sediment volume deposited in the Gulf ( $35 \text{ km}^3$ ). Based on this association, we assume that these suspended sediment fluxes are appropriate to use for each of the rivers we have sieved. We then derive the Holocene bedload flux for each river using the range of ratios of bedload to suspended loads, summarized in the previous subsection.

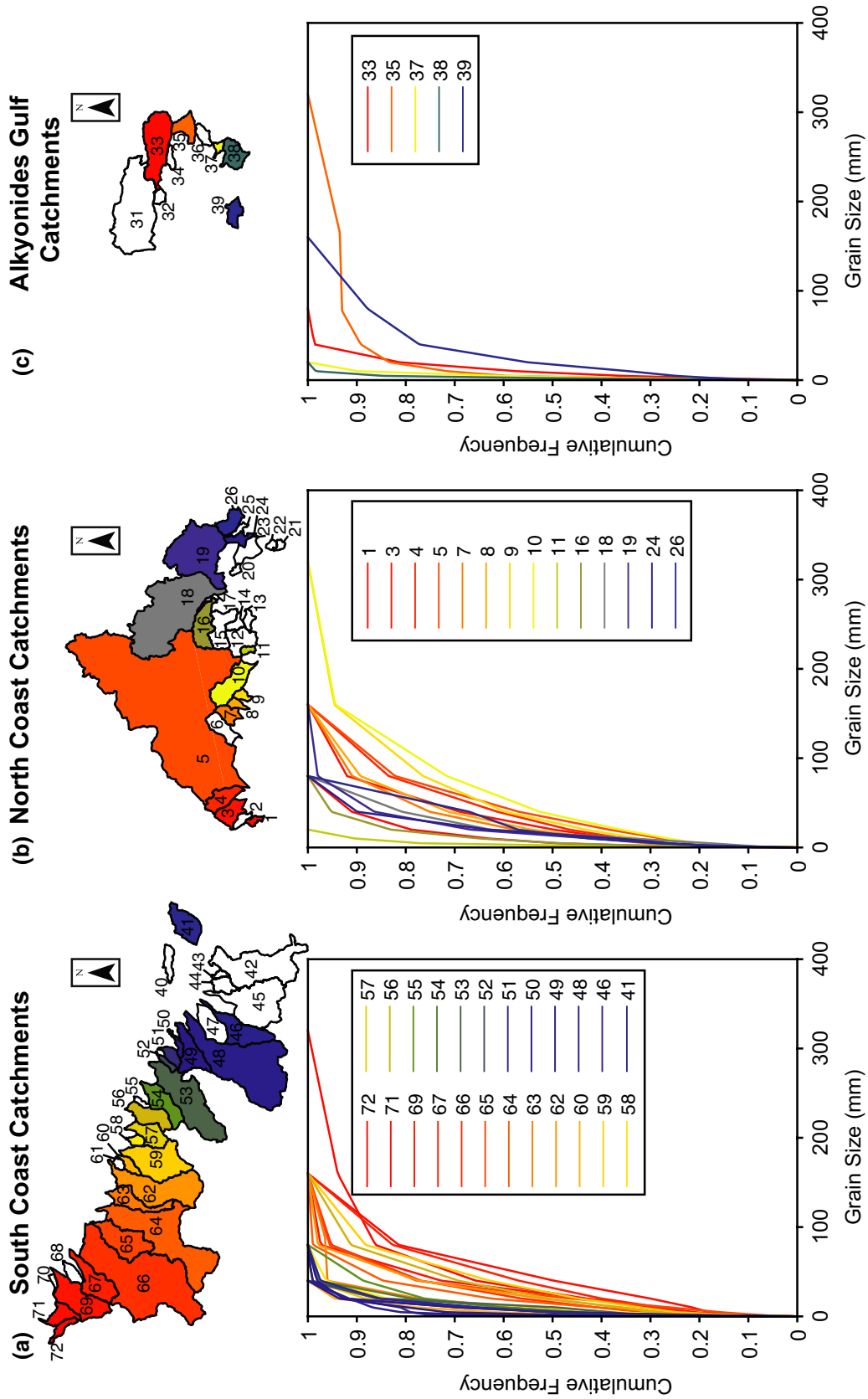


**FIGURE 4** Cumulative frequency plots of sieved grain-sizes, grouped into location around the coast: South coast (a), North coast (b) and Alkyonides Gulf (c). Catchments and respective cumulative frequency plots are colour coded with respect to an East-West red-blue colour spectrum

TABLE 1 Field collected data

Catchment name	Locality	Full weighted grain-size distribution (mm)		Grain-size distribution when greater 1 mm (mm)				Hydraulic geometries		
		Sieve		Wolman		Sieve		Bankfull width (m)	Bankfull height (m)	Slope (degrees)
		D <sub>50</sub>	D <sub>84</sub>	D <sub>50</sub>	D <sub>84</sub>	D <sub>50</sub>	D <sub>84</sub>			
1	1-1	5.1	28.4	12.5	26.1	8.8	33.6	5.5	1.5	0.4
2	2-1			40.8	152.0			9.2	1.0	2.9
3	3-1	20.2	66.1	33.2	72.3	29.5	71.0	19.2	0.8	0.8
4	4-1	24.6	82.5	43.9	98.2	35.3	94.6			0.8
5	5-1	32.5	88.1	51.9	90.0	38.7	96.4	88.6	2.7	2.2 <sup>a</sup>
6	7-1			47.5	111.0			26.1	1.7	1.5
7	8-1	15.3	62.4	42.1	100.0	20.9	69.4	16.3	1.8	1.5
8 <sup>b</sup>	9-1	17.0	68.3	86.0	286.0	22.5	72.9	25.6	1.2-1.4	4.8
9	10-1	28.3	113.0	33.3	90.0	36.7	123.0	11.8	0.5	1.8
10	12-1	36.8	123.0	32.0	72.4	48.1	131.0	24.0	1.2	0.9
11	13-1	2.4 <sup>c</sup>	7.5 <sup>c</sup>	10.7	44.0	3.3	8.8	6.1	1.0	1.1
16	18-1	5.3	21.5	31.6	69.4	8.1	26.2	12.1	0.5	2.4
18	20-2a	15.6	46.7	25.9	50.6	16.9	49.2	7.4	0.4	1 <sup>a</sup>
19	20-1a	13.3	37.6	30.0	45.8	15.8	39.6	6.5	0.7	0.9
20 <sup>b</sup>	21-1			109.0	206.0			16.4	0.9	6.7
23	24-4			40.4	69.9			7.6	1.3	1.8
24	25-1	15.1	35.6	22.0	52.5	17.5	37.1	6.5	0.5	1.0
26	27-1	15.2	60.6	56.0	96.3	18.4	62.4	3.4	0.7	2.8
33	33-1	8.2	23.1	23.1	43.2	9.0	24.3	22.7	1.8	0.3
35	35-1	3.8	22.2	19.7	50.6	4.4	28.9	4.7	1.1	3.5
37	37-1	3.7	9.0	6.8	13.4	4.6	9.5	3.1	1.0	1.9 <sup>a</sup>
38	38-1	2.2	4.7	4.7	8.3	3.0	6.0	8.5	1.0	0.7 <sup>a</sup>
39	39-1	17.5	65.6	18.5	50.6	20.1	72.0	3.9	2.1	0.3
41	42-1	4.7	19.3	12.7	35.0	8.7	23.7	7.9	1.0	1.1
46	46-1	0.8 <sup>d</sup>	7.4 <sup>d</sup>					11.7	1.0	2.4 <sup>a</sup>
48	48-1	5.3	16.5	20.6	40.8	7.4	17.6	12.5	1.3	0.3
49	49/50-1	2.0 <sup>d</sup>	13.1 <sup>d</sup>	11.5	20.6	4.2	17.2	15.0	1.4	2.9 <sup>a</sup>
50	51-1	4.8	16.3	19.8	36.4	6.6	17.2	8.2	1.2	0.7 <sup>a</sup>

(Continues)

TABLE 1 (Continued)

Catchment name	Locality	Full weighted grain-size distribution (mm)		Grain-size distribution when greater 1 mm (mm)				Hydraulic geometries		
		Sieve		Wolman		Sieve		Bankfull width (m)	Bankfull height (m)	Slope (degrees)
		$D_{50}$	$D_{84}$	$D_{50}$	$D_{84}$	$D_{50}$	$D_{84}$			
51	52-1a	0.2	12.6					7.0	1.2	2.9 <sup>a</sup>
52	53-1	4.6 <sup>d</sup>	19.1 <sup>d</sup>	19.7	44.0	9.8	24.1	24.9	1.2	1.3 <sup>a</sup>
53	54-1	10.3	19.7	26.1	42.6	14.4	25.2	18.0	1.9	0.8 <sup>a</sup>
54	55-1	6.5	25.4	14.2	33.2	10.8	29.3	28.0	1.5	0.6
55	56-1	6.4	32.5	20.0	43.3	10.2	37.7	4.4	1.3	4.1
56	57-1	19.4	66.9	29.7	67.0	28.0	71.6	7.5	1.8	0.7
57	58-1	4.3	18.0	10.3	24.5	8.7	19.9	29.4	1.3	0.8
58	59-1	8.9	20.2	17.4	39.6	11.3	24.0	5.9	0.9	3.0
59	60-1	25.8	73.4	53.4	91.7	31.3	75.9	10.3	2.0	0.1
60	61-1	2.8	13.7	12.1	26.5	5.6	16.6	5.2	0.8	0.6
62	63-1	18.7	53.0	24.8	54.1	23.9	57.4	126.2	0.5	0.7
63	64-1	7.5	26.9	25.9	38.6	12.4	30.7	6.9	1.0	1.5 <sup>a</sup>
64	65-2	14.2	39.4	39.1	73.2	17.0	43.6	23.8	0.6	0.7
65	67-1	22.3	54.0	26.9	61.4	24.1	56.1	58.2	1.2	1.0
66	68-1	15.9	55.5	38.5	90.0	20.2	60.1	27.4	0.9	0.1
67	70-1	31.8	86.2	33.3	78.1	39.2	95.4	55.8	<2	1.1
69	72-1	24.5	58.2	39.5	75.4	28.2	61.1	116.6	0.9	1.0
71	74-1	40.3	91.1	37.0	79.2	47.6	99.1	26.7	0.9	1.0
72	75-1	26.1	75.7	37.1	68.6	31.9	79.8	9.7	1.2	1.5

<sup>a</sup>Slope is taken at GPS location from DEM.

<sup>b</sup>Debris flow catchment.

<sup>c</sup>Sample taken in the field is 80% representative of full-weighted grain size distribution.

<sup>d</sup>Sample taken in the field is 95% representative of full-weighted grain size distribution.

We scaled the normalized sieved grain-size distribution at each site by the estimated Holocene bedload sediment flux for that river. We obtain a volume fraction for each grain-size class in each river, assuming the sieved grain-size data are representative of the transported bedload. We only consider the normalized volume that represents the grain-size distribution that is greater than 0.085 cm as this value corresponds to the suspended load-mixed load transition and smaller grain sizes are likely not transported in bedload at bankfull conditions (see Section 4.4). Finally, we sum the sediment flux corresponding to each grain-size bin for multiple rivers, which yields an estimate of the grain-size-specific Holocene bedload discharge (see Supporting Information for full description of this method).

## 4 | RESULTS

### 4.1 | Grain-size of sediment export to the Gulf

Figure 4 shows the cumulative frequency distributions of grain-size export from sieved data of gravel bars for 47 major rivers draining the Corinth Rift, divided into three sets based on location: the South coast of the Gulf of Corinth (Figure 4a); the North coast of the Gulf of Corinth (Figure 4b) and the Alkyonides Gulf (Figure 4c). As these distributions are measured at or near the river mouth we infer that this is what is being exported. Results indicate that the median grain-size export ( $D_{50}$ ) for the South coast is sand to pebble grade (finest  $D_{50}$  is 0.2 mm from catchment 51 in the East to a maximum of 40.3 mm from catchment 71 in the West). The sieved  $D_{84}$  varied from 19.3 mm in the East to 75.7 mm in the West (Figure 4a; Table 1). Only 12.5% of the measured  $D_{50}$  values along the South coast are sand grade or finer (<2 mm), and 21% of the  $D_{84}$  values are cobble grade (>64–256 mm). South coast catchments display a clear export trend, where finer grain-sizes are exported in the East (cooler colours; Figure 4a). In contrast, the North coast has a less clear trend. The sieved  $D_{50}$  ranges from 2.4 to 36.8 mm, and the range for  $D_{84}$  is 7.5 to 123 mm (Figure 4b; Table 1). Approximately 40% of  $D_{84}$  on the North coast are cobble grade (>64–256 mm) with the coarsest grain-size in the West part of the North coast. The largest  $D_{84}$  exported for the entire Gulf is 123 mm, corresponding to catchment 10 on the North coast (Figures 1 and 4b). The  $D_{50}$  and  $D_{84}$  along the Alkyonides Gulf range from 2.2 to 17.5 and 4.7 to 65.6 mm respectively (Figure 4c). The cumulative frequency distributions for every catchment draining the Corinth Rift exhibit the same unimodal distribution with median grain-sizes being within approximately a 40 mm range of one another. However, coarse-fraction  $D_{84}$  values exported to the Gulf have a range that is three times as large, covering

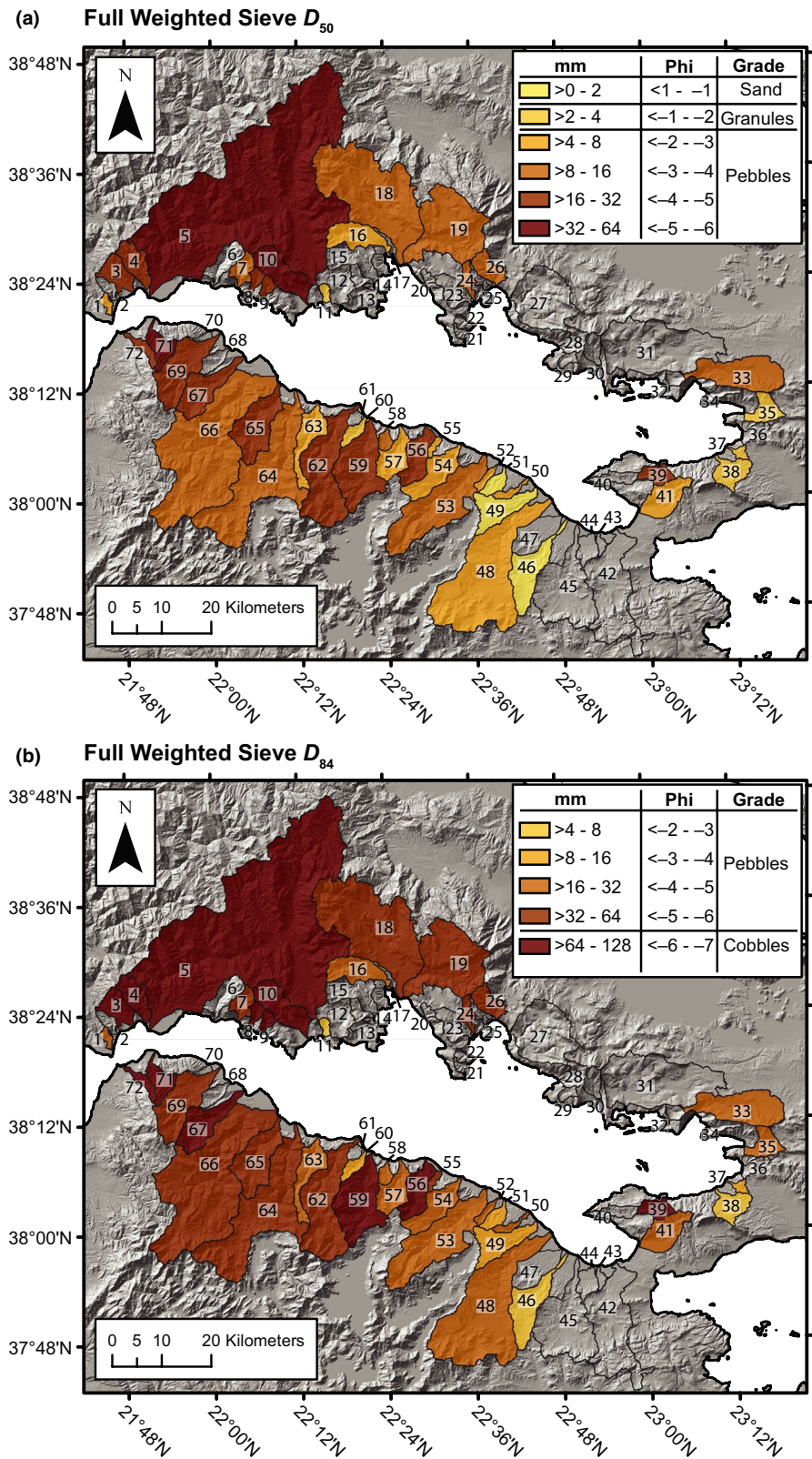
approximately 120 mm. The histograms of the raw sieved data can be found in the Supporting Information. These histograms reveal that the data are not normally distributed and as such  $D_{84}$  is not always one standard deviation from the median or mean grain size, however, Figure 4 reveals that the systematics of variation occur across a range of percentiles. Therefore, using the 84<sup>th</sup> percentile of the grain-size distribution for each catchment, consistent with previous studies (Brooke et al., 2018; Roda-Boluda et al., 2018) is valid when attempting to understand the causes of these variations. We note that we could have equally taken any high percentile value for comparison. Indeed, the higher the percentile the greater the spread in data and the clearer the variation between catchments.

The spatial trend in the  $D_{50}$  map (Figure 5a) highlights that fine-grained sediment ( $D_{50}$ , sand to the smallest pebble grade size, >2–8 mm) is exported at the eastern side of the South coast of the Gulf of Corinth (catchments 46 to 52), while rivers draining the central and western margins of the South coast Gulf of Corinth export coarser median grain-sizes (granule to coarsest pebble grade, >2–64 mm; catchments 53–72). Data also reveal a concentration of coarse  $D_{50}$  grain-size export (pebble grade, >16–32 mm; catchments 56, 59 and 62) in the centre of the South coast (Figure 5a). The coarsest  $D_{50}$  export for the entire rift is from the North-West coast and South-West coast, with three catchments, 71, 5 (the largest catchment—Mornos) and 10 (Figure 1), exporting the largest  $D_{50}$ .

The  $D_{84}$  map of grain-size transported from source catchments (Figure 5b) shows that for some catchments in the West of the Corinth Rift, the  $D_{84}$  found at river mouths is cobble grade (>64–128 mm, Figure 5b; catchments 3, 4, 5, 8, 9, 10, 67, 71 and 72). Similar to the  $D_{50}$  map, the coarsest  $D_{84}$  was measured from the central South coast, with catchments 56 and 59 exporting grain-sizes as large as 66.9 and 73.4 mm respectively (Table 1). In general, the coarse fraction of sediment ( $D_{84}$ ) exported from catchments along the eastern South coast (catchments 46 to 54) are markedly finer than the rest of the catchments along the South coast.

Figure 6 shows the comparison of the measured  $D_{50}$  and  $D_{84}$  grain-sizes from Wolman point count and in situ sieving. Grain-sizes less than 1 mm were excluded from the sieved data to enable a one to one comparison. Although these methods are measuring different aspects of the same channel bars and therefore not truly equivalent, we wish to explore if the Wolman point count method can give a good representation of the subsurface when fines of less than 1 mm are excluded. This is especially important in areas where sieving is not possible. Wolman  $D_{50}$  and sieved  $D_{50}$  grain-sizes exhibit a strong positive correlation with a linear regression slope of 1.22 (Figure 6a), indicating that the Wolman median grain-sizes are approximately 20% coarser when compared to their sieved counterpart.

**FIGURE 5** Catchment colour-coded with respect to their sieved  $D_{50}$  (a) and  $D_{84}$  exports (b). The  $D_{50}$  and  $D_{84}$  for each catchment are placed into categories that correspond to the legend in the figure where each category has a millimetre measurement, phi measurement and a descriptive term. The colours darken with increasing grain-size



Similarly, Wolman  $D_{84}$  and sieved  $D_{84}$  also show a positive relationship. In this case the slope of the linear regression line is approximately 1, indicating good agreement between the methods, although the Wolman  $D_{84}$  underestimates the in

situ-sieved  $D_{84}$  in catchments with the coarsest grain-sizes ( $\sim 90$  mm; Figure 6b). Nevertheless, the datasets indicate that the Wolman point count provides a good first-order measure of gravel bar grain-size when sieving is not practicable.

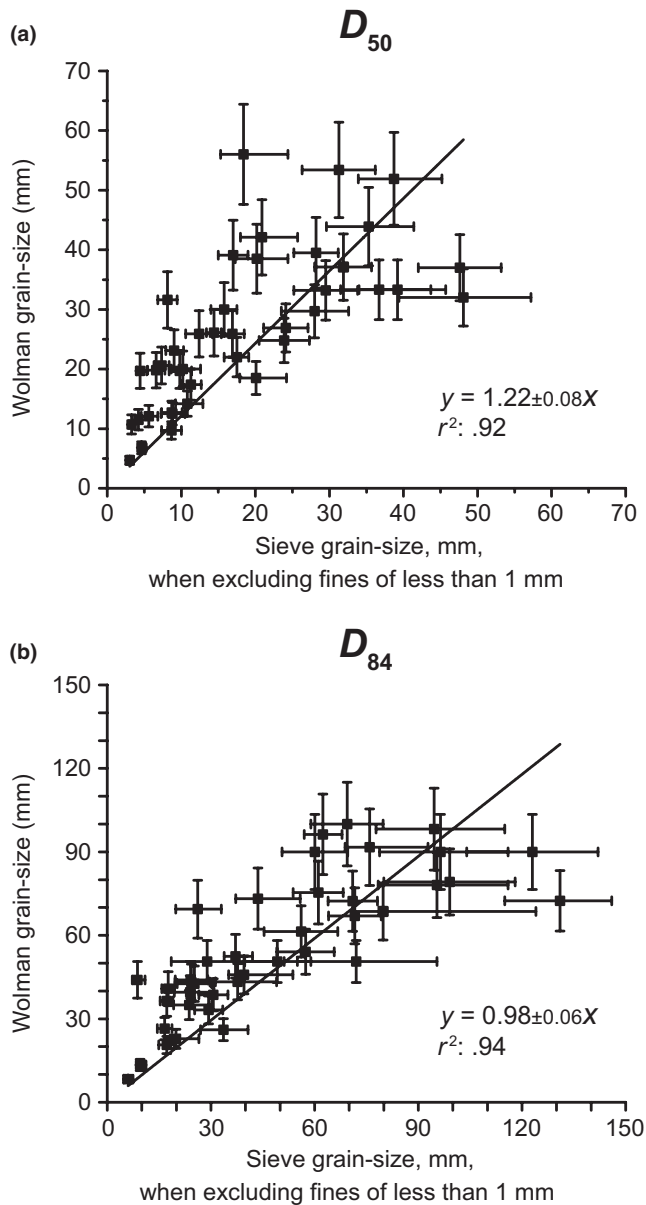


**FIGURE 6** (a) Comparison of Wolman point count  $D_{50}$  with sieved  $D_{50}$  (when excluding fines of less than 1 mm). Wolman point count error bars are  $\pm 15\%$  and sieve error bars denote  $D_{45}$ – $D_{55}$ . (b) Comparison of Wolman point count  $D_{84}$  with sieved  $D_{84}$  (when excluding fines of less than 1 mm). Wolman point count error bars are  $\pm 15\%$  and sieve error bars denote  $D_{79}$ – $D_{89}$

## 4.2 | What factors control grain-size?

In this section, we investigate the controls on the final grain-size export from the catchments into the Corinth Rift. We begin by testing the role that geomorphic and hydrologic parameters play in controlling grain-size exported from the Corinth rivers.

### 4.2.1 | Geomorphic and hydrologic parameters

Following related studies on upland rivers in the Andes and the Swiss Alps (Litty & Schlunegger, 2017; Litty et al., 2017), we compared our sieved  $D_{50}$  and  $D_{84}$  across the catchments with their respective catchment area, maximum catchment relief, percentage of catchment area with slopes greater than 30 degrees and mean annual precipitation rate (Figure 7). Figure 7 shows the (a) fitted linear model with the corresponding  $r^2$  value and (b) corresponding  $t$  statistic for the slope of the linear model (Figure 7).

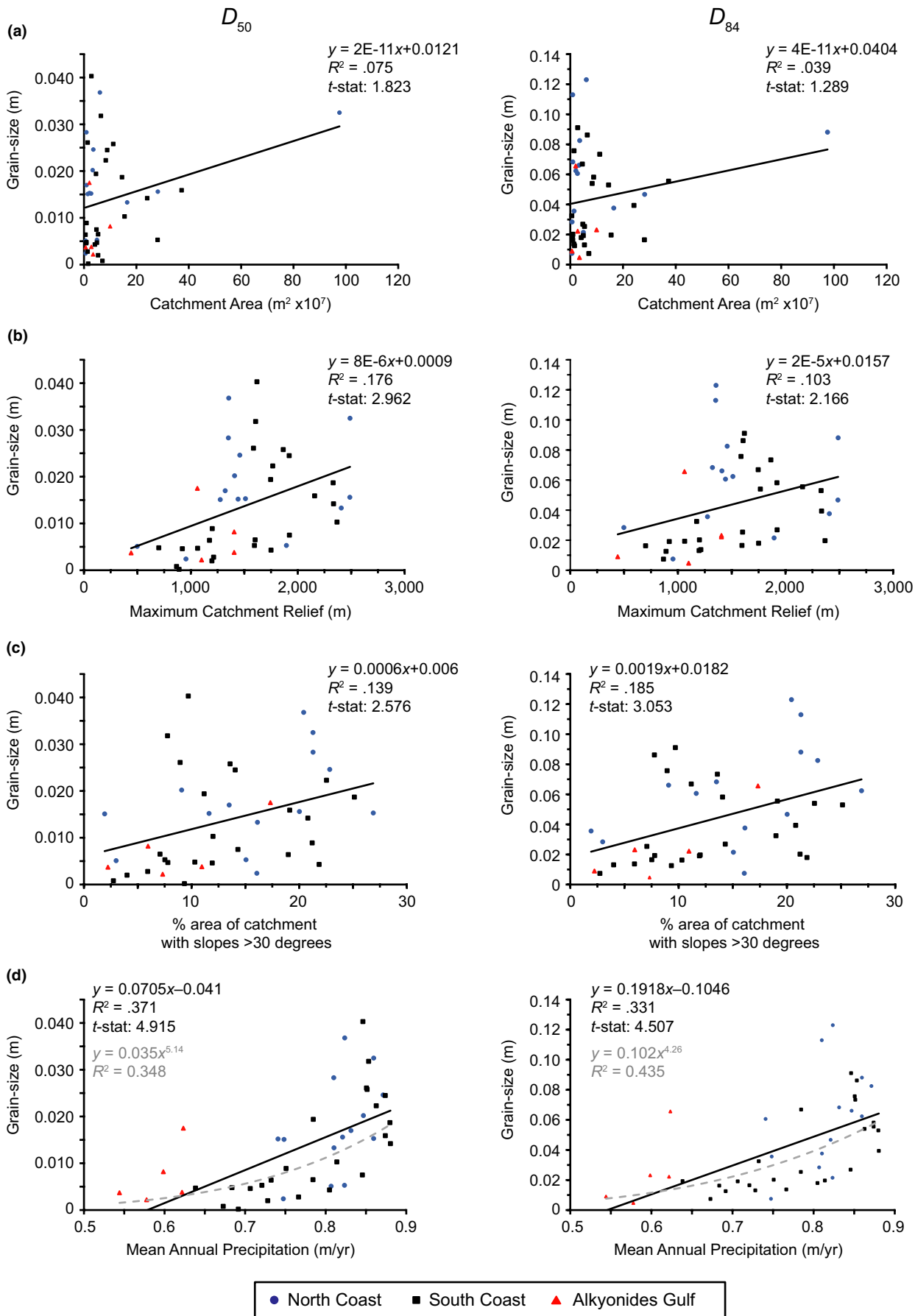
Our analysis revealed that the measured  $D_{50}$  and  $D_{84}$  data did not exhibit a linear relationship with catchment area (Figure 7a), and the computed  $r^2$  values were low ( $D_{50}$ : 0.08,  $D_{84}$ : 0.04; Figure 7a) and  $t$  statistics ( $D_{50}$ : 1.82,  $D_{84}$ : 1.29; Figure 7a) were less than the critical value at the 95% significance level ( $\pm 2.101$ ). In contrast, the measured  $D_{50}$  and  $D_{84}$  exhibited a linear trend with the (a) maximum catchment relief (Figure 7b) and (b) percentage of area of catchment with slopes  $>30$  degrees (Figure 7c), with the estimated  $t$  statistics greater than that of the critical value at the 95% significance level. However, the  $r^2$  value of the linear relationships were  $<.2$  (Figure 7b,c), indicating that less than 20% of the variance in grain-size data is explained by a linear relationship with respect to slope and relief.

Finally, our analysis revealed that  $D_{50}$  and  $D_{84}$  are correlated with the mean annual precipitation ( $MAP$ ; Figure 7d), with wetter catchments being associated with larger median and coarse-fraction grain sizes. A linear regression suggests: (a)  $D_{50} = 0.0705 * MAP - 0.04$ ,  $r^2$  of .37, and (b)  $D_{84} = 0.192 * MAP - 0.11$ ,  $r^2$  of .33 (Figure 7d); in both cases the  $r^2$  of these relationships are greater than the others in Figure 7. The computed  $t$  statistic in both these cases exceeds the critical value at a significance level of 95%, thus leading to the rejection of the null hypothesis that the regression slope is zero. We found that a power-law model between  $D_{84}$  and precipitation has an even greater  $r^2$  value (.44), suggesting that a non-linear relationship may better capture the trends between the grain-size exported from the catchments and  $MAP$  (Figure 7d).

### 4.2.2 | Lithological and tectonic controls

Previous work has shown that bedrock lithology and tectonic uplift rates may control the grain-size export from catchments (Allen et al., 2015; Roda-Boluda et al., 2018;

**FIGURE 7** Sieved  $D_{50}$  and  $D_{84}$  plotted against a series of geomorphic and hydrological parameters including: Catchment area (a), Maximum catchment relief (b), Percentage of catchment with slopes greater than  $30^\circ$  (c) and Catchment mean annual precipitation,  $MAP$ , mm/year (d). Black squares denote South coast catchments, blue circles denote North coast catchments and red triangles denote catchments draining into the Alkyonides Gulf



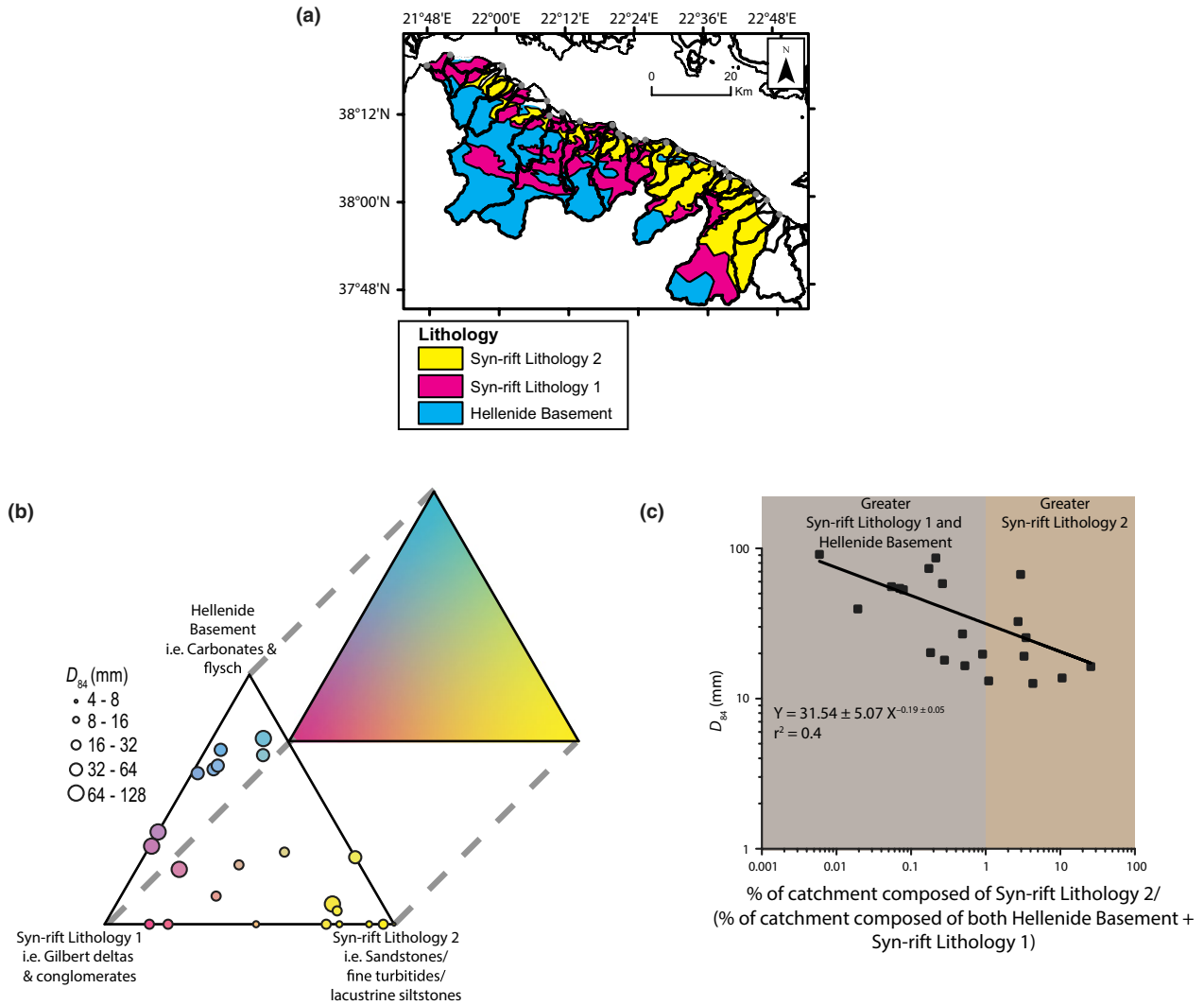


**FIGURE 8** (a) The simplified lithological map of the South coast (seen also in Figure 2); (b) A ternary diagram where each apex represents a catchment draining a 100% of either Hellenide Basement, Syn-rift Lithology 1 or Syn-rift Lithology 2, then the  $D_{84}$  of the southern catchments are plotted depending on their respective catchments lithology and scaled for their export size and; (c) A plot showing the percentage of each catchment composed of Syn-rift Lithology 2 divided by the combination of Hellenide Basement and Syn-rift Lithology 1 plotted against their respective  $D_{84}$  export. Values >1 on the x-axis represent catchments that have relatively more Syn-rift Lithology 2 and <1 represents catchments that have relatively more Hellenide Basement and Syn-rift Lithology 1. The plot clearly shows that an increase in Syn-rift Lithology 2 within catchment areas results in a reduction in the size of  $D_{84}$

Whittaker et al., 2010). To test for lithological controls on grain-size export in our study area, we made a Cyan-Magenta-Yellow (CMY) ternary diagram (Figure 8b), based on the lithological grouping outlined in the Section 3.2, in which the exported  $D_{84}$  from the South coast catchments are plotted with respect to percentage of the three main lithologies present within these catchments (Figures 2 and 8a). Each  $D_{84}$  grain-size point is coloured based on the catchment lithology composition in the CMY ternary plot. Figure 8b reveals that the larger points, that is larger 84<sup>th</sup> percentile grain-sizes, are associated with catchments that have relatively higher contributions of Hellenide Basement and Syn-rift Lithology 1 (Gilbert-type deltas/conglomerates) and as a result are coloured cyan to magenta. In contrast, the majority of the smaller points, which relate to relatively smaller  $D_{84}$ ,

are predominantly associated with catchments composed primarily of Syn-rift Lithology 2 (sandstones/siltstones/mudstones; yellow; Figure 8b). To further elucidate this relationship, we compared the measured  $D_{84}$  against the ratio of the percentage of Syn-rift Lithology 2 and the combined percentage of Hellenide Basement and Syn-rift Lithology 1 present within their respective catchment (Figure 8c). A ratio value less than 1 corresponds to catchment with higher fraction of the Hellenide Basement and Syn-rift Lithology 1, and a ratio value greater than 1 indicates dominance of more Syn-rift Lithology 2 within the catchment (Figure 8c). We find a negative correlation exists between the sieved  $D_{84}$  measurements for each catchment and the ratio of the percentage of Syn-rift Lithology 2 and the combined percentage of Hellenide Basement and Syn-rift Lithology 1 present within

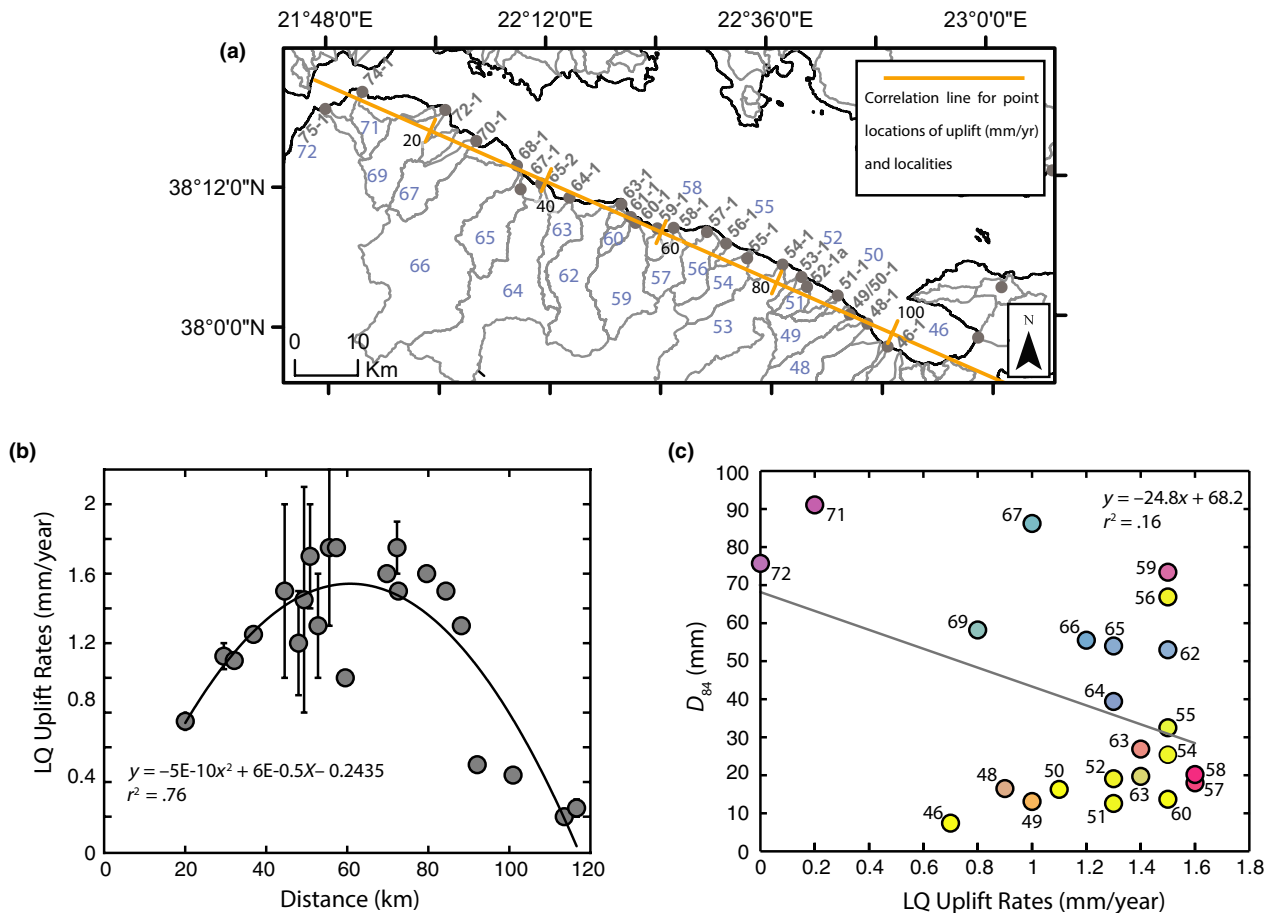


**FIGURE 9** (a) Map of the South coast of the Gulf of Corinth, catchments are labelled in blue, sample sites are grey spots. A yellow line denotes the line to which uplift rates in Figure 1-inset are correlated to. (b) Late Quaternary (LQ) uplift rates from Figure 1-inset, compiled by Pechlivanidou et al. (2019), plotted along-strike the yellow line in (a). (c)  $D_{84}$  from each sample site in (a) plotted against late Quaternary uplift rates that were extrapolated from the trendline in (b). Each point is colour coded depending on the sample site location within the ternary diagram seen in (b). All points have their respective catchment label

each catchment (Figure 8c). This observation suggests that catchments composed predominantly of Hellenide Basement and Syn-rift Lithology 1 have coarser export than catchments composed primarily of Syn-rift Lithology 1.

To test the influence of tectonics on grain-size, we plotted the late Quaternary uplift rates (Figure 1-inset; Pechlivanidou et al., 2019) for the sample sites along the South coast relative to their location along the line shown in Figure 9a. A polynomial fit was used to parameterize the distribution of uplift rates to first-order (Figure 9b), which were then compared to our sieved  $D_{84}$  measurements (Figure 9c).

When  $D_{84}$  is plotted against late Quaternary uplift rates we find a negative linear trend, where only 16% of the variance in  $D_{84}$  is explained by a linear relationship (Figure 9c). For instance while uplift rates are highest in the centre of the South coast (50–80 km; Figure 9b;  $r^2 = .76$ ), the coarsest measured  $D_{84}$  is not located here (Figure 9c), which suggests that there is no simple relationship between tectonically driven uplift rates and grain-size exported. However, when we colour code the  $D_{84}$  points with respect to their

location in the ternary diagram (Figure 8b) and thus consider catchment lithology, potential trends emerge. For instance, relatively fine  $D_{84}$  clasts (<40 mm) in Figure 9c span a wider range of uplift rates (0.6–1.6 mm/year). However, these points are predominantly coloured yellow and thus are derived from catchments that are composed predominantly of Syn-rift Lithology 2 (sandstones/siltstones/mudstones). In fact, there appears to be a slight increase in  $D_{84}$  with uplift rates when solely considering the yellow (Syn-rift Lithology 2) points. This suggests that lithology exerts a greater effect on grain-sizes than tectonics. Similarly, coarser  $D_{84}$  clasts (>40 mm) are associated with catchments that have a lithology dominated by the Hellenide Basement (cyan coloured markers in Figure 9c) and uplift rates estimated here are of a similar range as those catchments that export finer  $D_{84}$ . In summary, finer  $D_{84}$  measurements are associated with Syn-rift Lithology 2 and coarser  $D_{84}$  measurements are associated more with Hellenide Basement and Syn-rift Lithology 1 lithologies. Furthermore, when data from the catchments that are dominated by the Syn-rift

Lithology 2 alone are considered, then the  $D_{84}$  increases with increasing uplift rate (Figure 9c).

### 4.3 | What is the mode of sediment transport?

The ratio of the settling velocity to shear velocity computed for  $D_{84}$  and  $D_{50}$  indicate that the primary mode of transport for the sediment we sampled near the river mouths is bedload for the majority of the rivers draining into the Gulf (Figure 10); the cumulative frequency curve shows that ~64% of the measured  $D_{84}$  and ~14% of the  $D_{50}$  reside in the bedload-dominated regime. Our results indicate that the median and coarse fractions of the grain-size distributions measured are primarily transported in bedload and mixed load (i.e. intermittent suspension). At bankfull conditions, the estimated  $W_s/u_*$  for both the  $D_{50}$  and  $D_{84}$  values do not reside in the suspended transport regime for all the catchments studied here (Figure 10). In contrast, results indicate that fine sand is transported predominantly as suspended load at bankfull conditions (Figure 10).

### 4.4 | Total Corinth Rift Holocene sediment budget

Figure 11 reveals the total Holocene sediment budget for the entire Corinth Rift. We find that the median grain-size at the threshold of suspension (i.e.  $W_s/u_* = 0.3$ ; Figure 10) is 0.083 cm. We

interpret this result to indicate that the majority of the suspended of the suspended volume is comprised of grain-sizes that span 0–0.085 cm, and the bedload volume is primarily comprised of grain-sizes within the range of 0.085–32 cm (Figure 11).

Results indicate that the total bedload volume, estimated from the measured Holocene suspended sediment volume in the Gulf, 18.8 km<sup>3</sup>, using a bedload to suspended load ratio of 35:65 (Pratt-Sitaula et al., 2007). The upper and lower bounds on the total bedload volume were 25.6 and 11.7 km<sup>3</sup>, using bedload to suspended ratios of 45:55 and 25:75 (Turowski et al., 2010) respectively.

### 4.5 | Grain-size-specific bedload discharge for the Holocene

We use bedload fluxes that are derived from BQART suspended discharges exported for the 43 sieved rivers from Watkins et al. (2018) to produce the Holocene grain-size-specific bedload discharge in Figure 12. We find that the Holocene grain-size-specific sediment discharge is approximately 21% (i.e. 2 km<sup>3</sup>) coarse sand to granule grade sediment, 0.085–0.4 cm (bins 0.085–0.475 cm; Figure 12). Around 79% (approximately 7.4 km<sup>3</sup>) is between 0.475 and 16 cm, approximately pebble to cobble grade (Figure 12). The dominant contributing grain-size fractions are both within the 1–2 and 2–4 cm bins, with approximately 21% in both (1.96 and 1.91 km<sup>3</sup> respectively; Figure 12; medium pebble to very large pebble, 0.8–6.4 cm). The grain-size

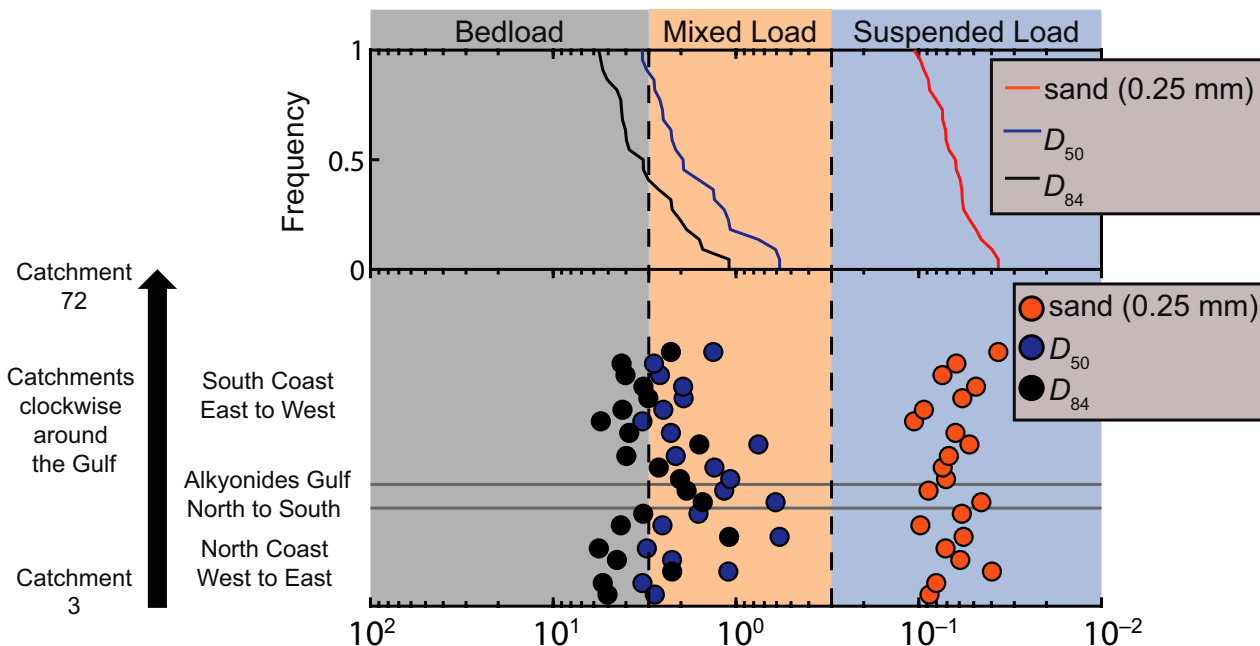


**FIGURE 10** Shows two sets of results; (i—lower graph)  $W_s/u_*$  calculated using  $D_{50}$  (blue circles),  $D_{84}$  (black circles) and medium-fine sand (0.25 mm; orange circles) for 22 of the catchments (see Supporting Information), and; (ii—upper graph) cumulative frequency of  $D_{50}$  (blue line),  $D_{84}$  (black line) and medium-fine sand (orange line). For the sake of clarity, bedload, mixed-load and suspended-load transport regimes are highlighted with clear boundaries at  $W_s/u_* = 3$  and 0.3 (Dade & Friend, 1998)

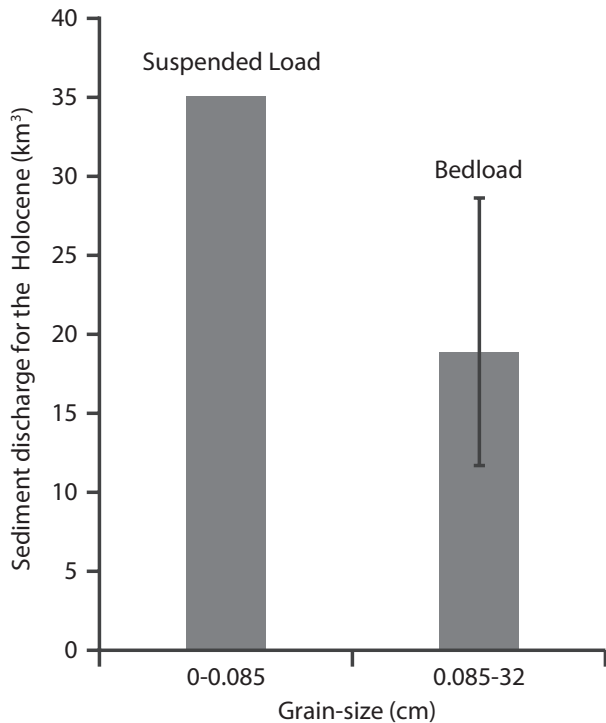


**FIGURE 11** The suspended and bedload Holocene volumes for the entire rift. Suspended volume comes from Watkins et al. (2018) seismically derived Holocene volume (35 km<sup>3</sup>). Bedload volume is derived using a ratio of 35:65 bedload to suspended load. Upper and lower bedload error bars are based off bedload to suspended load ratios of 45:55 and 25:75 respectively

fraction of 16–32 cm contributes the least to the bedload sediment budget, approximately 0.2% (0.02 km<sup>3</sup>).

We find that the total bedload discharge for the Holocene, when deriving from suspended BQART estimations and applying the 35:65 bedload to suspended load ratio is 9.4 km<sup>3</sup> (note that the value when derived from seismic data in Figure 11 is 18.8 km<sup>3</sup>). We, however, are not concerned by the disparity of these numbers because we know that the total BQART suspended load volume is lower than the observed volume, 35 km<sup>3</sup>; from Watkins et al. (2018). We also infer that the shape of the Holocene grain-size bedload sediment discharge distribution in Figure 12 would not change if the unaccounted-for catchments were added because they are spatially scattered around the Gulf of Corinth and these catchments are unlikely to be characterized by different grain-size dynamics than the rest of the catchments studied here.

## 5 | DISCUSSION

### 5.1 | Comparison of grain-size from in situ sieving versus Wolman point counts

We sieved approximately 3 tonnes of sediment to constrain the full-weighted grain-size distribution exported at the

mouths of 47 rivers, accounting for ~83% of the Corinth Rift by area. In situ sieving allows for the characterization of the full-weighted grain-size distribution of a sedimentary deposit, but many studies instead use the Wolman point count method to characterize the surface grain-size distribution >1 mm of modern sediments (i.e. no fine sediment; for example Brooke et al., 2018; Roda-Boluda et al., 2018). We find that point count data can adequately, but not perfectly, reproduce median and coarse fraction grain-sizes obtained from gravel bars by in situ sieving when the fines of the sieved sediment are excluded. Sieving characterizes the *b* (intermediate) axis of clasts; however, our modified Wolman point count captures the *a* (long) axis. We show that this approach produces reasonable results (Figure 6), even though the *a* axis is systematically larger than the *b* axis. Previous studies (Litty et al., 2017) have shown that the ratio of the long to intermediate axis is relatively constant implying that the trend in the correlation would be unaffected. Our results indicate that Wolman point count data capture the full-weighted grain-size distribution reasonably well provided the information on the finer fraction of distribution is not required. These results therefore lend support to previous studies that have solely undertaken point counts without sieving to characterize the grain-size distribution (e.g., D'Arcy, Whittaker, & Roda-Boluda, 2016; Litty & Schlunegger, 2017; Roda-Boluda et al., 2018). However, complete sediment budgets (including fines <1 mm) cannot be calculated without sieving, and our study highlights the importance of considering the full-weighted grain-size distribution to fully characterize grain-size distribution ( $D_{50}$  and  $D_{84}$ ).

### 5.2 | Controls on grain-size export within the Corinth Rift

This is the first study where the bedload grain-size export distribution for an entire rift has been constrained. The cumulative frequency graphs show that marked variations in grain-size export around the Gulf exist (Figure 4). We showed from our analysis that catchment area has no statistical control on grain-sizes (Figure 7a). For the other geomorphic parameters, our results suggest that the (a) maximum catchment relief (Figure 7b) and (b) percentage of catchment with areas greater than 30 degrees (Figure 7c), exhibit a linear trend with measured grain size, albeit with low  $r^2$  values suggesting that little of the variance in grain-size can be explained by these variables. In contrast, we find that  $D_{50}$  and  $D_{84}$  demonstrably vary with mean annual precipitation rate (a proxy for discharge) for both linear and power law models, with the latter displaying a stronger relationship (Figure 7d). These results are consistent with the idea that higher precipitation rates lead to higher water discharges that result in the mobilization

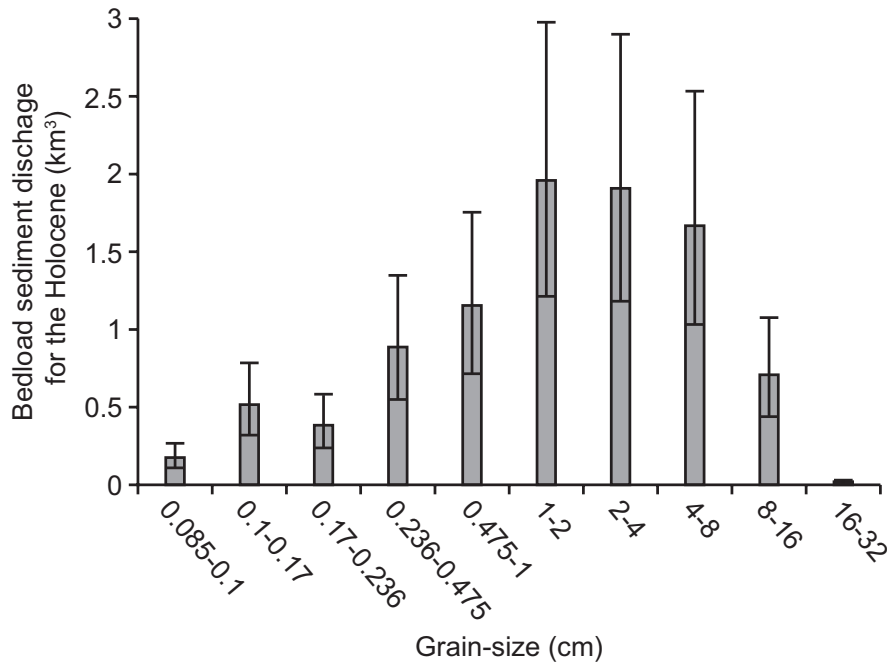


**FIGURE 12** The Holocene grain-size-specific bedload discharge for the Corinth Rift. The bars are when a 35:65 bedload to suspended load ratio is assumed and the upper and lower error bars are when we assume a bedload to suspended load ratios of 45:55 and 27:75 respectively

of larger clasts, supporting similar findings from the Andean catchments (Litty et al., 2017). We theorize this observation may reflect the role of storms at the sub-catchment scale, given that a similar correlation with grain-size does not apply to catchment drainage area.

Our results demonstrate that the catchment lithology exerts a clear influence on the final grain-size distributions exported from the catchments (Figure 8). Catchments that drain predominantly Hellenide Basement (Carbonates and Flysch) and Syn-rift Lithology 1 (Gilbert deltas and conglomerates) have a coarser sediment export than catchments that predominantly drain the Syn-rift Lithology 2 (sandstones/siltstones/mudstones; Figure 8b,c). Given that Syn-rift Lithology 2 is a weaker substrate compared to other lithological units in the study area, we infer that catchments dominated by this bedrock lithology may supply finer input sediment distributions from the hillslopes to the river network (cf. Allen et al., 2015; Roda-Boluda et al., 2018). In addition, disparate rates of fluvial abrasion for different constituent lithologies may also explain the trends observed in our data. Previous laboratory experiments have revealed that fluvial abrasion rates can be up to 500 times higher for unconsolidated sandstones than for stronger metamorphic lithologies like quartzite (Attal & Lavé, 2009); however, these experiments also showed significant scatter for a given lithology that was attributed to factors such as silification of sandstones, schistosity planes, content of phyllic minerals and mixture of different grain-size lithologies within the bedload flux (Attal & Lavé, 2009). In our analysis, we distilled the local lithologies into three broad groups (Figure 8) and the observed lithological control on the grain-size export may be more apparent because of spatial averaging at a regional scale. Regardless, our data are

consistent with previous observations that catchments with weak bedrock lithologies may export finer sediment because of both high rates of fluvial abrasion and finer input grain-size distributions from the hillslopes to the fluvial network. Future work will be needed to address which specific lithological parameters (e.g., rock strength, degree of jointing, cementation etc.) are most important for controlling grain size release from catchments. Furthermore, we acknowledge that one of the units consists of uplifted Gilbert delta conglomerates so there is the possibility of recycling of clasts (e.g., Sinclair, Stuart, Mudd, McCann, & Tao, 2019). In order for this to be quantified further a full lithological examination of these deposits would be required.

Our results also indicate that uplift rates alone have little control on the final grain-size distribution released from rivers on the South coast of the Gulf of Corinth (Figure 9c). However, when we introduce the colours pertaining to catchment lithology from Figure 8 into the  $D_{84}$  against late Quaternary uplift rates graph (Figure 9c), we observe that the finer  $D_{84}$  (<40 mm) are predominantly yellow in colour (Syn-rift Lithology 2) and appear to be weakly yet positively correlated with late Quaternary uplift rates (Figure 9c). This suggests that tectonics does have an influence on grain-size, but catchment lithologies need to be accounted for to detect this signal. This finding is in contrast to previous studies that showed that long-term tectonic uplift rates significantly affect the grain-size (Pechlivanidou et al., 2018; Roda-Boluda et al., 2018; Whittaker et al., 2010). Whittaker et al. (2010) hypothesized that coarse sediment found within knickzones of catchments being uplifted by active normal faults was a result of increased landsliding due to slope-steepening. Roda-Boluda et al. (2018) also documented increased landsliding frequency

within knickzones, but they demonstrated that the grain-size supplied by landslides was highly dependent on the underlying lithology. Together, these findings suggest that while the transient response of the catchments along the South coast of Gulf of Corinth to Quaternary uplift (Demoulin, Beckers, & Hubert-Ferrari, 2015) may cause increased landsliding within the knickzones (cf. Roda-Boluda et al., 2018; Whittaker et al., 2010), it is the underlying lithology that governs the calibre of grain-size input from landslides (cf. Roda-Boluda et al., 2018) and modulates how susceptible the input grain-size is to abrasion once it enters the fluvial transport realm.

Measurements of grain-size from catchments with the highest late Quaternary uplift rates further bolster our interpretation that bedrock lithology acts as a primary control on grain-size export at the regional scale. For example catchments 50 to 55 along the Corinth South coast have high uplift rates ( $>1.1$  mm/year, Figure 9c) but do not correspond to the coarsest grain-size export. Instead, these catchments (50 to 55) are dominated by Syn-rift Lithology 2 lithology, which we argue yields finer grain-size distributions when compared to catchments with Hellenide Basement lithology (cf. Roda-Boluda et al., 2018). The finer input grain-size distribution can then be more readily abraded once they enter the river system (cf. Attal & Lavé, 2009). We therefore caution against the simplistic interpretation that higher uplift rates can result in coarser sediment export into a basin at the regional scale, because the underlying lithology may exert the dominant control on grain-size export with a secondary tectonic signal superimposed (Figure 9c).

### 5.3 | Grain-size-specific bedload budget and implications for the resulting basin architecture

Our results have significant implications for sediment delivery, basin architecture and facies partitioning within the Gulf of Corinth depocentre. Using channel hydraulics and sediment transport theory, we showed that the median and coarse-fraction of the grain-size distributions measured here are predominantly exported as bedload under bankfull flow conditions (Figure 10). The resulting bedload sediment budget, the first for any rift system, shows that 79% of the bedload is pebble grade and coarser (Figure 12) and the remaining 21% is coarse sand to granule grade (Figure 12). The presence of Gilbert-type deltas, that fringe much of the coast, coupled with new borehole data indicating that the main basin is predominantly composed of muds and silts (McNeill et al., 2019), suggests that (a) the constrained bedload sediment budget is deposited at the coast and does not reach the main basin floor, and for many source catchments this sediment may be entirely sequestered in the their Holocene Gilbert delta or associated proximal

turbidite systems (cf. Cullen, Collier, Gawthorpe, Hodgson, & Barrett, 2019); (b) for rivers that do not have large deltas, the bedload is likely mostly trapped on the shelf. Our results also confirm that sediment  $<0.085$  cm, that is medium sand, fine sand, silts and mud grade sediments are exported primarily as suspended load in bankfull conditions (Figure 10). This fine fraction of the total sediment load is likely mobilized more frequently than the median and coarse fraction of the grain-size distribution, even in flows below the bankfull stage. Thus, sand, silt and mud grade sediment may have a shorter residence time in the fluvial transport realm when compared to bedload fraction ( $>0.085$  cm) of the grain-size distribution, which is likely the reason why only 8% of the total amount that we have sieved resides in suspended load as it is much more easily mobilized and exported. Observations also indicate that fine sediment can be delivered to the basin readily through hypopycnal flows (Beckers et al., 2016). The disparate source-to-sink transfer timescales for coarse and fine fraction of the sediment suggests that these grain-size fractions can be partitioned differently within the basin architecture of the Corinth Rift. These observations may also be pertinent to other rift systems such as the Gulf of Suez (Young, Gawthorpe, & Sharp, 2003) and the North Sea (van Cappelle, Ravnås, Hampson, & Johnson, 2017).

Our results also have implications for the interpretation of rifting/faulting and sediment supply from the basin architecture. To date, studies have largely focussed on the locus and magnitude of sediment supply (Armitage, Jones, Duller, Whittaker, & Allen, 2013; Cowie et al., 2006; Gawthorpe & Leeder, 2000; Watkins et al., 2018) and the variations in  $D_{50}$  and  $D_{84}$  when investigating basin stratigraphy (e.g., Armitage et al., 2011; Brooke et al., 2018). Our study highlights the importance of considering the full grain-size distribution supplied by the catchments and the relative timescales over which different fractions of the grain-size distribution reside within the fluvial transport zone before being stored within basins. The inferred long timescales of transit for the median and coarse sediment supply suggests that tectonic, climatic and lithological signals expressed within the grain-size distribution may be attenuated or lost due to the fluvial morphodynamics over timescales shorter than the fluvial sediment storage timescales (Ganti et al., 2014; Jerolmack & Paola, 2010; Romans et al., 2016). However, allogenic signals expressed in the grain-size distribution may be recorded within the sedimentary record when the transfer timescales of the sediment from source to sink are shorter than the associated climatic or tectonic perturbations (Ganti et al., 2014; Jerolmack & Paola, 2010), consistent with previous studies that documented tectonic and lithological controls on grain-size released from upland catchments on million year timescales (Allen et al., 2015; Roda-Boluda et al., 2018; Whittaker et al., 2010).

Our investigation of  $D_{84}$  export with respect to uplift (Figure 9c) suggests that, on the regional scale, sedimentary basin architecture may not retain a grain-size-specific tectonic signal because of multiple constituent lithologies. We conclude that catchment lithology is the primary determinant of grain-size supplied to the basin in the Corinth Rift. Results indicate that this is likely a consequence of lithological controls on both the input grain-size distribution supplied from hillslopes and landslides and the sediment abrasion properties. Many catchments along the southern coast have knickpoints at varying locations (Demoulin et al., 2015) and future work could investigate how the location of knickzones with respect to active faults and river mouths dictates grain-size supply to the upstream river network (cf. Roda-Boluda et al., 2018; Whittaker et al., 2010), and how quickly this signal is lost, for instance by down-system abrasion (Attal & Lavé, 2009; Dingle et al., 2017). We argue that a wide range of grain-sizes may be yielded in time and space if a rift is studied at the regional scale spanning multiple lithologies and with catchments in different stages of response to active faulting, which complicates the simplistic interpretation of basin stratigraphy as a function of rift evolution (Gawthorpe & Leeder, 2000).

## 6 | CONCLUSIONS

We constrained, for the first time, the full-weighted bedload grain-size export for an entire rift. Based on extensive field measurements of the grain-size distributions at the mouths of 47 rivers draining into the Gulf of Corinth, combined with data of the composition of the bedrock lithology, late Quaternary uplift rates, geomorphic and hydrologic parameters, and sediment transport theory, we find that:

- A clear grain-size export trend exists along the South coast of the Gulf of Corinth, where finer  $D_{84}$  grain-size is exported to the East, with values as low as 7.4 mm. The measured bedload grain-size distributions coarsen westward and reach a maximum  $D_{84}$  of ~91 mm in the catchments that are farthest West of the rift.
- The median and 84<sup>th</sup> percentiles of the grain-size distributions estimated using Wolman point counts reasonably, but not perfectly, match those estimated using in situ sieving (when excluding fines of <1 mm). However, in the absence of constraints on the fine fraction of the grain-size distribution through in situ sieving, it is not possible to fully quantify the full grain-size distribution by this method.
- Bedrock lithology, rather than tectonic uplift rate, exerts the dominant control on final-grain-size distributions measured at the river mouths. Finer grain-sizes are associated with weaker bedrock, possibly because catchments with weak bedrock both supply finer input grain-size distribution

from landslides and may also be readily abraded during fluvial transport. For a given bedrock lithology, the exported grain-size shows a weak positive correlation with the late Quaternary uplift rates, suggesting a secondary tectonic control on grain-size export into the rift.

- The median and coarse fraction of the measured grain-sizes are predominantly transported as bedload and intermittent suspension at bankfull conditions. In contrast, medium and fine sand, silt and mud may be readily mobilized and transported predominantly as suspended load for the same flow conditions, suggesting disparate timescales of transit for fine and coarse fraction of sediment being supplied to the basin. This observation provides a mechanistic explanation for the facies partitioning seen in the modern Corinth Rift basin architecture where large relatively coarse-grained Gilbert-type deltas fringe much of the Gulf and fine sediments dominate the basin fill (McNeill et al., 2019; Moretti et al., 2004).
- The bedload sediment budget of the rift is primarily composed of pebble grade and coarser sediment, and we infer that this sediment budget corresponds to the Gilbert-type deltas that fringe much of the Gulf of Corinth with the suspended sediment load primarily contributing to the sediment budget of the main basin depocentre.
- Together, our results demonstrate how the interplay between bedrock lithology, tectonics, climate and fluvial morphodynamics may manifest in the grain-size export signal at the rift scale with implications for controls on basin architecture and for inferring paleoenvironmental changes from the sedimentary record.

## ACKNOWLEDGEMENTS

This research was funded by the Imperial College Janet Watson bursary, the Natural Environment Research Council (NERC) Science and Solutions for a Changing Planet Doctoral Training Partnership support to Watkins, a Royal Society grant RG 140109 to Bell and Whittaker, a Swiss National Fund (SNF) grant N°200020\_182017 and a VISTA Scholarship. We thank the editor Cari Johnson and the reviewers, Hugh Sinclair, Fritz Schlunegger and an anonymous reviewer for their insightful reviews on a previous version of the manuscript. We also thank Sofia Pechlivanidou and Patience Cowie for their comments on the discussion and Thomas Sheldrake for his help regarding the statistical analysis. Furthermore, we thank the National Cadastre & Mapping Agency S.A. for the use of their 5 m DEM.

## DATA AVAILABILITY STATEMENT

The data that support the findings of this study are provided in the Supporting Information. Raw data that support the findings of this study are available from the corresponding author upon reasonable request.

## ORCID

Stephen E. Watkins  <https://orcid.org/0000-0003-1916-0584>

Alexander C. Whittaker  <https://orcid.org/0000-0002-8781-7771>

Rebecca E. Bell  <https://orcid.org/0000-0002-4785-9707>

Robert L. Gawthorpe  <https://orcid.org/0000-0002-4352-6366>

Lisa C. McNeill  <https://orcid.org/0000-0002-8689-5882>

## REFERENCES

- Allen, P. A. (2008). From landscapes into geological history. *Nature*, 451(7176), 274–276. <https://doi.org/10.1038/nature06586>
- Allen, P. A., Armitage, J. J., Carter, A., Duller, R. A., Michael, N. A., Sinclair, H. D., ... Whittaker, A. C. (2013). The Qs problem: Sediment volumetric balance of proximal foreland basin systems. *Sedimentology*, 60(1), 102–130. <https://doi.org/10.1111/sed.12015>
- Allen, P. A., Armitage, J. J., Whittaker, A. C., Michael, N. A., Roda-Boluda, D., & D'Arcy, M. (2015). Fragmentation model of the grain size mix of sediment supplied to basins. *The Journal of Geology*, 123(5), 405–427. <https://doi.org/10.1086/683113>
- Allen, P. A., & Densmore, A. (2000). Sediment flux from an uplifting fault block. *Basin Research*, 12(3–4), 367–380. <https://doi.org/10.1111/j.1365-2117.2000.00135.x>
- Armijo, R., Meyer, B., King, G., Rigo, A., & Papanastassiou, D. (1996). Quaternary evolution of the Corinth Rift and its implications for the Late Cenozoic evolution of the Aegean. *Geophysical Journal International*, 126(1), 11–53. <https://doi.org/10.1111/j.1365-246X.1996.tb05264.x>
- Armitage, J. J., Allen, P. A., Burgess, P. M., Hampson, G. J., Whittaker, A. C., Duller, R. A., & Michael, N. A. (2015). Sediment transport model for the Eocene Escanilla sediment-routing system: Implications for the uniqueness of sequence stratigraphic architectures. *Journal of Sedimentary Research*, 85(12), 1510–1524. <https://doi.org/10.2110/jsr.2015.97>
- Armitage, J. J., Duller, R. A., Whittaker, A. C., & Allen, P. A. (2011). Transformation of tectonic and climatic signals from source to sedimentary archive. *Nature Geoscience*, 4(4), 231–235. <https://doi.org/10.1038/NNGEO1087>
- Armitage, J. J., Jones, T. D., Duller, R. A., Whittaker, A. C., & Allen, P. A. (2013). Temporal buffering of climate-driven sediment flux cycles by transient catchment response. *Earth and Planetary Science Letters*, 369, 200–210. <https://doi.org/10.1016/j.epsl.2013.03.020>
- Attal, M., & Lavé, J. (2009). Pebble abrasion during fluvial transport: Experimental results and implications for the evolution of the sediment load along rivers. *Journal of Geophysical Research: Earth Surface*, 114(F4). <https://doi.org/10.1029/2009JF001328>
- Attal, M., Mudd, S., Hurst, M., Weinman, B., Yoo, K., & Naylor, M. (2015). Impact of change in erosion rate and landscape steepness on hillslope and fluvial sediments grain size in the Feather River basin (Sierra Nevada, California). *Earth Surface Dynamics*, 3(1), 201–222. <https://doi.org/10.5194/esurf-3-201-2015>
- Avallone, A., Briole, P., Agatza-Balodimou, A. M., Billiris, H., Charade, O., Mitsakaki, C., ... Veis, G. (2004). Analysis of eleven years of deformation measured by GPS in the Corinth Rift Laboratory area. *Comptes Rendus Geoscience*, 336(4–5), 301–311. <https://doi.org/10.1016/j.crte.2003.12.007>
- Backert, N., Ford, M., & Malartre, F. (2010). Architecture and sedimentology of the Kerinitis Gilbert-type fan delta, Corinth Rift, Greece. *Sedimentology*, 57(2), 543–586. <https://doi.org/10.1111/j.1365-3091.2009.01105.x>
- Bagnold, R. A. (1966). An approach to the sediment transport problem from general physics. US Geol. Survey Prof. Paper 422-I, Washington, D.C.
- Beckers, A., Beck, C., Hubert-Ferrari, A., Tripsanas, E., Crouzet, C., Sakellariou, D., ... De Batist, M. (2016). Influence of bottom currents on the sedimentary processes at the western tip of the Gulf of Corinth, Greece. *Marine Geology*, 378, 312–332. <https://doi.org/10.1016/j.margeo.2016.03.001>
- Bell, R., McNeill, L. C., Bull, J., Henstock, T., Collier, R., & Leeder, M. (2009). Fault architecture, basin structure and evolution of the Gulf of Corinth Rift, central Greece. *Basin Research*, 21(6), 824–855. <https://doi.org/10.1111/j.1365-2117.2009.00401.x>
- Bornovas, I., & Rondogianni-Tsiambaou, T. H. (1983). *Geological map of Greece* (2nd edn.), 1:500,000 scale, Athen, Greece: Institute of Geology and Mineral Exploration.
- Briole, P., Rigo, A., Lyon-Caen, H., Ruegg, J., Papazissi, K., Mitsakaki, C., ... Deschamps, A. (2000). Active deformation of the Corinth rift, Greece: results from repeated Global Positioning System surveys between 1990 and 1995. *Journal of Geophysical Research: Solid Earth*, 105(B11), 25605–25625. <https://doi.org/10.1029/2000JB900148>
- Brooke, S. A. S., Whittaker, A. C., Armitage, J. J., D'Arcy, M., & Watkins, S. E. (2018). Quantifying sediment transport dynamics on alluvial fans from spatial and temporal changes in grain size, Death Valley, California. *Journal of Geophysical Research: Earth Surface*, 123(8), 2039–2067. <https://doi.org/10.1029/2018JF004622>
- Cassel, E. J., & Graham, S. A. (2011). Paleovalley morphology and fluvial system evolution of Eocene-Oligocene sediments (“auriferous gravels”), northern Sierra Nevada, California: Implications for climate, tectonics, and topography. *Geological Society of America Bulletin*, 123(9–10), 1699–1719. <https://doi.org/10.1130/B30356.1>
- Clarke, P. J., Davies, R. R., England, P. C., Parsons, B. E., Billiris, H., Paradissis, D., ... Bingley, R. (1997). Geodetic estimate of seismic hazard in the Gulf of Korinthos. *Geophysical Research Letters*, 24(11), 1303–1306. <https://doi.org/10.1029/97GL01042>
- Clarke, P. J., Davies, R. R., England, P. C., Parsons, B., Billiris, H., Paradissis, D., ... Briole, P. (1998). Crustal strain in central Greece from repeated GPS measurements in the interval 1989–1997. *Geophysical Journal International*, 135(1), 195–214. <https://doi.org/10.1046/j.1365-246X.1998.00633.x>
- Cowie, P., Attal, M., Tucker, G., Whittaker, A., Naylor, M., Ganas, A., & Roberts, G. (2006). Investigating the surface process response to fault interaction and linkage using a numerical modelling approach. *Basin Research*, 18(3), 231–266. <https://doi.org/10.1111/j.1365-2117.2006.00298.x>
- Cullen, T. M., Collier, R. E. L., Gawthorpe, R. L., Hodgson, D. M., & Barrett, B. J. (2019). Axial and transverse deep-water sediment supply to syn-rift fault terraces: Insights from the West Xylokastrou Fault Block, Gulf of Corinth, Greece. *Basin Research*. <https://doi.org/10.1111/bre.12416>
- Dade, W. B., & Friend, P. F. (1998). Grain-size, sediment-transport regime, and channel slope in alluvial rivers. *The Journal of Geology*, 106(6), 661–676. <https://doi.org/10.1086/516052>
- Damm, B., Becht, M., Varga, K., & Heckmann, T. (2010). Relevance of tectonic and structural parameters in Triassic bedrock formations to landslide susceptibility in Quaternary hillslope sediments. *Quaternary International*, 222(1–2), 143–153. <https://doi.org/10.1016/j.quaint.2010.02.022>

- D'Arcy, M., Roda-Boluda, D. C., & Whittaker, A. C. (2017). Glacial-interglacial climate changes recorded by debris flow fan deposits, Owens Valley, California. *Quaternary Science Reviews*, *169*, 288–311. <https://doi.org/10.1016/j.quascirev.2017.06.002>
- D'Arcy, M., Whittaker, A. C., & Roda-Boluda, D. C. (2016). Measuring alluvial fan sensitivity to past climate changes using a self-similarity approach to grain-size fining, Death Valley, California. *Sedimentology*, *64*(2), 388–424. <https://doi.org/10.1111/sed.12308>
- De Martini, P. M., Pantosti, D., Palyvos, N., Lemeille, F., McNeill, L., & Collier, R. (2004). Slip rates of the Aigion and Eliki faults from uplifted marine terraces, Corinth Gulf, Greece. *Comptes Rendus Geoscience*, *336*(4), 325–334. <https://doi.org/10.1016/j.crte.2003.12.006>
- De Wever, P. (1975). Etude géologique des séries apparaissent en fenêtre sous l'allochtone pindique (série de Tripolitza et série épimétamorphique de Zaroukla) Péloponnèse septentrionale, Grèce. *Thèse 3e cycle*. Université de Lille, France.
- Degnan, P. J., & Roberston, A. H. F. (1998). Mesozoic–early Tertiary passive margin evolution of the Pindos ocean (NW Peloponnese, Greece). *Sedimentary Geology*, *117*(1–2), 33–70. [https://doi.org/10.1016/S0037-0738\(97\)00113-9](https://doi.org/10.1016/S0037-0738(97)00113-9)
- Demoulin, A., Beckers, A., & Hubert-Ferrari, A. (2015). Patterns of Quaternary uplift of the Corinth rift southern border (N Peloponnese, Greece) revealed by fluvial landscape morphometry. *Geomorphology*, *246*, 188–204. <https://doi.org/10.1016/j.geomorph.2015.05.032>
- Densmore, A. L., Allen, P. A., & Simpson, G. (2007). Development and response of a coupled catchment fan system under changing tectonic and climatic forcing. *Journal of Geophysical Research: Earth Surface*, *112*(F1), 2003–2012. <https://doi.org/10.1029/2006JF000474>
- Dercourt, J. (1964). Contribution à l'étude géologique d'un secteur du Péloponnèse septentrional. *Annales Géologiques Des Pays, Helleniques*, *15*, 418.
- Dingle, E. H., Attal, M., & Sinclair, H. D. (2017). Abrasion-set limits on Himalayan gravel flux. *Nature*, *544*, 471. <https://doi.org/10.1038/nature22039>
- Duller, R. A., Whittaker, A. C., Swinehart, J. B., Armitage, J. J., Sinclair, H. D., Bair, A., & Allen, P. A. (2012). Abrupt landscape change post–6 Ma on the central Great Plains, USA. *Geology*, *40*(10), 871–874. <https://doi.org/10.1130/G32919.1>
- Ferguson, R. I., & Church, M. (2004). A simple universal equation for grain settling velocity. *Journal of Sedimentary Research*, *74*(6), 933–937. <https://doi.org/10.1306/051204740933>
- Ferguson, R., Hoey, T., Wathen, S., & Werritty, A. (1996). Field evidence for rapid downstream fining of river gravels through selective transport. *Geology*, *24*(2), 179–182. [https://doi.org/10.1130/0091-7613\(1996\)024%3C0179:FEFRDF%3E2.3.CO;2](https://doi.org/10.1130/0091-7613(1996)024%3C0179:FEFRDF%3E2.3.CO;2)
- Ferguson, R., Prestegard, K., & Ashworth, P. (1989). Influence of sand on hydraulics and gravel transport in a braided gravel bed river. *Water Resources Research*, *25*(4), 635–643. <https://doi.org/10.1029/WR025i004p00635>
- Ford, M., Hemelsdaël, R., Mancini, M., & Palyvos, N. (2016). Rift migration and lateral propagation: Evolution of normal faults and sediment-routing systems of the western Corinth rift (Greece). *Geological Society, London, Special Publications*, *439*(1), 131–168. <https://doi.org/10.1144/SP439.15>
- Ford, M., Rohais, S., Williams, E. A., Bourlange, S., Jousset, D., Backert, N., & Malartre, F. (2013). Tectono-sedimentary evolution of the western Corinth rift (Central Greece). *Basin Research*, *25*(1), 3–25. <https://doi.org/10.1111/j.1365-2117.2012.00550.x>
- Ford, M., Williams, E. A., Malartre, F., Popescu, S. M., & Nichols, G. (2007). Stratigraphic architecture, sedimentology and structure of the Vouraikos Gilbert-type fan delta, Gulf of Corinth, Greece. *Sedimentary Processes, Environments and Basins: A Tribute to Peter Friend*, *38*, 49–90.
- Forzoni, A., Storms, J. E., Whittaker, A. C., & Jager, G. (2014). Delayed delivery from the sediment factory: Modeling the impact of catchment response time to tectonics on sediment flux and fluvio-deltaic stratigraphy. *Earth Surface Processes and Landforms*, *39*(5), 689–704. <https://doi.org/10.1002/esp.3538>
- Ganti, V., Lamb, M. P., & McElroy, B. (2014). Quantitative bounds on morphodynamics and implications for reading the sedimentary record. *Nature Communications*, *5*, 3298. <https://doi.org/10.1038/ncomms4298>
- Garefalakis, P., & Schlunegger, F. (2018). Link between concentrations of sediment flux and deep crustal processes beneath the European Alps. *Scientific Reports*, *8*(183), 1–11. <https://doi.org/10.1038/s41598-017-17182-8>
- Gawthorpe, R., & Leeder, M. (2000). Tectono-sedimentary evolution of active extensional basins. *Basin Research*, *12*(3–4), 195–218. <https://doi.org/10.1111/j.1365-2117.2000.00121.x>
- Gawthorpe, R. L., Leeder, M. R., Kranis, H., Skourtsos, E., Andrews, J. E., Henstra, G. A., ... Stamatakis, M. (2018). Tectono-sedimentary evolution of the Plio-Pleistocene Corinth rift. *Greece. Basin Research*, *30*(3), 448–479. <https://doi.org/10.1111/bre.12260>
- Glaus, G., Delunel, R., Stutenbecker, L., Akçar, N., Christl, M., & Schlunegger, F. (2019). Differential erosion and sediment fluxes in the Landquart basin and possible relationships to lithology and tectonic controls. *Swiss Journal of Geosciences*, *112*, 453–473. <https://doi.org/10.1007/s00015-019-00344-3>
- Guzzetti, F., Cardinali, M., & Reichenbach, P. (1996). The influence of structural setting and lithology on landslide type and pattern. *Environmental & Engineering Geoscience*, *2*(4), 531–555. <https://doi.org/10.2113/gsegeosci.II.4.531>
- Hampson, G. J., Duller, R. A., Petter, A. L., Robinson, R. A., & Allen, P. A. (2014). Mass-balance constraints on stratigraphic interpretation of linked Alluvial–Coastal–Shelfal deposits from source to sink: Example from Cretaceous Western Interior Basin, Utah and Colorado, USA. *Journal of Sedimentary Research*, *84*(11), 935–960. <https://doi.org/10.2110/jsr.2014.78>
- Hellenic National Cadastre and Mapping Agency S.A. (2016). 5 meter Digital Elevation Model. Athens: The National Cadastre and Mapping Agency S.A.
- Hijmans, R. J., Cameron, S. E., Parra, J. L., Jones, P. G., & Jarvis, A. (2005). Very high resolution interpolated climate surfaces for global land areas. *International Journal of Climatology: A Journal of the Royal Meteorological Society*, *25*(15), 1965–1978. <https://doi.org/10.1002/joc.1276>
- Houghton, S. L., Roberts, G. P., Papanikolaou, I. D., McArthur, J. M., & Gilmour, M. A. (2003). New 234U–230Th coral dates from the western Gulf of Corinth: Implications for extensional tectonics. *Geophysical Research Letters*, *30*(19). <https://doi.org/10.1029/2003GL018112>
- Jerolmack, D. J., & Paola, C. (2010). Shredding of environmental signals by sediment transport. *Geophysical Research Letters*, *37*(19). <https://doi.org/10.1029/2010GL044638>
- Kellerhals, R., & Bray, D. I. (1971). Sampling procedures for coarse fluvial sediments. *Journal of the Hydraulics Division*, *97*(8), 1165–1180.
- Keraudren, B., & Sorel, D. (1987). The terraces of Corinth (Greece)—A detailed record of eustatic sea-level variations during the last

- 500,000 years. *Marine Geology*, 77(1–2), 99–107. [https://doi.org/10.1016/0025-3227\(87\)90085-5](https://doi.org/10.1016/0025-3227(87)90085-5)
- Komar, P., & Shih, S.-M. (1992). Equal mobility versus changing bedload grain sizes in gravel-bed streams. In P. Billi, R. D. Hey, C. R. Thorne, & P. Tacconi (Eds.), *Dynamics of gravel-bed rivers* (pp. 73–93). Chichester, UK: Wiley.
- Lamb, M. P., Nittrouer, J. A., Mohrig, D., & Shaw, J. (2012). Backwater and river plume controls on scour upstream of river mouths: Implications for fluvio-deltaic morphodynamics. *Journal of Geophysical Research: Earth Surface*, 117(F1). <https://doi.org/10.1029/2011JF002079>
- Le Pichon, X., Chamot-Rooke, N., Lallemand, S., Noomen, R., & Veis, G. (1995). Geodetic determination of the kinematics of central Greece with respect to Europe: Implications for Eastern Mediterranean tectonics. *Journal of Geophysical Research*, 100(B7), 12675–12690.
- Leeder, M. R., Harris, T., & Kirkby, M. J. (1998). Sediment supply and climate change: Implications for basin stratigraphy. *Basin Research*, 10(1), 7–18. <https://doi.org/10.1046/j.1365-2117.1998.00054.x>
- Leopold, L. B., & Wolman, M. G. (1957). *River channel patterns: Braided, meandering, and straight*. Washington: US Government Printing Office.
- Litty, C., & Schlunegger, F. (2017). Controls on Pebbles' size and shape in streams of the Swiss Alps. *The Journal of Geology*, 125(1), 101–112. <https://doi.org/10.1086/689183>
- Litty, C., Schlunegger, F., & Viveen, W. (2017). Possible threshold controls on sediment grain properties of Peruvian coastal river basins. *Earth Surface Dynamics*, 5(3), 571. <https://doi.org/10.5194/esurf-5-571-2017>
- Margielewski, W. (2006). Structural control and types of movements of rock mass in anisotropic rocks: Case studies in the Polish Flysch Carpathians. *Geomorphology*, 77(1–2), 47–68. <https://doi.org/10.1016/j.geomorph.2006.01.003>
- McClusky, S., Balassanian, S., Barka, A., Demir, C., Ergintav, S., Georgiev, I., ... Kahle, H. (2000). Global Positioning System constraints on plate kinematics and dynamics in the eastern Mediterranean and Caucasus. *Journal of Geophysical Research: Solid Earth*, 105(B3), 5695–5719. <https://doi.org/10.1029/1999JB900351>
- McNeill, L. C., & Collier, R. L. (2004). Uplift and slip rates of the eastern Eliki fault segment, Gulf of Corinth, Greece, inferred from Holocene and Pleistocene terraces. *Journal of the Geological Society*, 161(1), 81–92. <https://doi.org/10.1144/0016-764903-029>
- McNeill, L. C., Collier, R. L., De Martini, P., Pantosti, D., & D'Addezio, G. (2005). Recent history of the Eastern Eliki Fault, Gulf of Corinth: Geomorphology, palaeoseismology and impact on palaeoenvironments. *Geophysical Journal International*, 161(1), 154–166. <https://doi.org/10.1111/j.1365-246X.2005.02559.x>
- McNeill, L. C., Cotterill, C., Bull, J., Henstock, T., Bell, R., & Stafatos, A. (2007). Geometry and slip rate of the Aigion fault, a young normal fault system in the western Gulf of Corinth. *Geology*, 35(4), 355–358. <https://doi.org/10.1130/G23281A.1>
- McNeill, L. C., Shillington, D. J., Carter, G. D. O., Everest, J. D., Gawthorpe, R. L., Miller, C., ... Green, S. (2019). High-resolution record reveals climate-driven environmental and sedimentary changes in an active rift. *Scientific Reports*, 9(1). <https://doi.org/10.1038/s41598-019-40022-w>
- Michael, N. A., Whittaker, A. C., Carter, A., & Allen, P. A. (2014). Volumetric budget and grain-size fractionation of a geological sediment routing system: Eocene Escanilla Formation, south-central Pyrenees. *Geological Society of America Bulletin*, 126(3–4), 585–599. <https://doi.org/10.1130/B30954.1>
- Moretti, I., Lykousis, V., Sakellariou, D., Reynaud, J.-Y., Benziene, B., & Prinzhofer, A. (2004). Sedimentation and subsidence rate in the Gulf of Corinth: What we learn from the Marion Dufresne's long-piston coring. *Comptes Rendus Geoscience*, 336(4), 291–299. <https://doi.org/10.1016/j.crte.2003.11.011>
- Mouyaris, N., Papastamatiou, D., & Vita-Finzi, C. (1992). The Helice Fault? *Terra Nova*, 4(1), 124–128. <https://doi.org/10.1111/j.1365-3121.1992.tb00457.x>
- Nixon, C. W., McNeill, L. C., Bull, J. M., Bell, R. E., Gawthorpe, R. L., Henstock, T. J., ... Kranis, H. (2016). Rapid spatio-temporal variations in rift structure during development of the Corinth Rift, central Greece. *Tectonics*, 35(5), 1225–1248. <https://doi.org/10.1002/2015TC004026>
- Ori, G. G. (1989). Geologic history of the extensional basin of the Gulf of Corinth (?Miocene-Pleistocene). *Greece. Geology*, 17(10), 918–921. [https://doi.org/10.1130/0091-7613\(1989\)017%3C0918:GHOTEB%3E2.3.CO;2](https://doi.org/10.1130/0091-7613(1989)017%3C0918:GHOTEB%3E2.3.CO;2)
- Paola, C., & Mohrig, D. (1996). Palaeohydraulics revisited: Palaeoslope estimation in coarse-grained braided rivers. *Basin Research*, 8(3), 243–254. <https://doi.org/10.1046/j.1365-2117.1996.00253.x>
- Parsons, A. J., Michael, N. A., Whittaker, A. C., Duller, R. A., & Allen, P. A. (2012). Grain-size trends reveal the late orogenic tectonic and erosional history of the south-central Pyrenees, Spain. *Journal of the Geological Society*, 169(2), 111–114. <https://doi.org/10.1144/0016-76492011-087>
- Pechlivanidou, S., Cowie, P. A., Duclaux, G., Nixon, C. W., Gawthorpe, R. L., & Salles, T. (2019). Tipping the balance: Shifts in sediment production in an active rift setting. *Geology*, 47(3), 259–262. <https://doi.org/10.1130/G45589.1>
- Pechlivanidou, S., Cowie, P. A., Hannisdal, B., Whittaker, A. C., Gawthorpe, R. L., Pennos, C., & Riiser, O. S. (2018). Source-to-sink analysis in an active extensional setting: Holocene erosion and deposition in the Sperchios rift, central Greece. *Basin Research*, 30(3), 522–543. <https://doi.org/10.1111/bre.12263>
- Perissoratis, C., Piper, D., & Lykousis, V. (2000). Alternating marine and lacustrine sedimentation during late Quaternary in the Gulf of Corinth rift basin, central Greece. *Marine Geology*, 167(3), 391–411. [https://doi.org/10.1016/S0025-3227\(00\)00038-4](https://doi.org/10.1016/S0025-3227(00)00038-4)
- Pirazzoli, P., Stiros, S., Arnold, M., Laborel, J., Laborel-Deguen, F., & Papageorgiou, S. (1994). Episodic uplift deduced from Holocene shorelines in the Perachora Peninsula, Corinth area, Greece. *Tectonophysics*, 229(3), 201–209. [https://doi.org/10.1016/0040-1951\(94\)90029-9](https://doi.org/10.1016/0040-1951(94)90029-9)
- Pratt-Sitaula, B., Garde, M., Burbank, D. W., Oskin, M., Heimsath, A., & Gabet, E. (2007). Bedload-to-suspended load ratio and rapid bedrock incision from Himalayan landslide-dam lake record. *Quaternary Research*, 68(1), 111–120. <https://doi.org/10.1016/j.yqres.2007.03.005>
- Rădoane, M., Rădoane, N., Dumitriu, D., & Miclăuș, C. (2008). Downstream variation in bed sediment size along the East Carpathian rivers: Evidence of the role of sediment sources. *Earth Surface Processes and Landforms*, 33(5), 674–694. <https://doi.org/10.1002/esp.1568>
- Roberts, S., & Jackson, J. (1991). Active normal faulting in central Greece: An overview. In A. M. Roberts, G. Yielding, & B. Freeman (Eds.), *The Geometry of Normal Faults: Geological Society, London, Special Publication*, (vol. 56, pp. 125–142). <https://doi.org/10.1144/GSL.SP.1991.056.01.09>
- Roda-Boluda, D. C., D'Arcy, M., McDonald, J., & Whittaker, A. C. (2018). Lithological controls on hillslope sediment supply: Insights

- from landslide activity and grain size distributions. *Earth Surface Processes and Landforms*, 43(5), 956–977. <https://doi.org/10.1002/esp.4281>
- Rohais, S., Eschard, R., Ford, M., Guillocheau, F., & Moretti, I. (2007). Stratigraphic architecture of the Plio-Pleistocene infill of the Corinth Rift: Implications for its structural evolution. *Tectonophysics*, 440(1–4), 5–28. <https://doi.org/10.1016/j.tecto.2006.11.006>
- Romans, B. W., Castellort, S., Covault, J. A., Fildani, A., & Walsh, J. (2016). Environmental signal propagation in sedimentary systems across timescales. *Earth-Science Reviews*, 153, 7–29. <https://doi.org/10.1016/j.earscirev.2015.07.012>
- Sinclair, H. D., Gibson, M., Naylor, M., & Morris, R. G. (2005). Asymmetric growth of the Pyrenees revealed through measurement and modeling of orogenic fluxes. *American Journal of Science*, 305(5), 369–406. <https://doi.org/10.2475/ajs.305.5.369>
- Sinclair, H. D., Stuart, F. M., Mudd, S. M., McCann, L., & Tao, Z. (2019). Detrital cosmogenic <sup>21</sup>Ne records decoupling of source-to-sink signals by sediment storage and recycling in Miocene to present rivers of the Great Plains, Nebraska, USA. *Geology*, 47(1), 3–6. <https://doi.org/10.1130/G45391.1>
- Skourlis, K., & Doutsos, T. (2003). The Pindos Fold-and-thrust belt (Greece): Inversion kinematics of a passive continental margin. *International Journal of Earth Sciences*, 92(6), 891–903. <https://doi.org/10.1007/s00531-003-0365-4>
- Skourtsos, E., & Kranis, H. (2009). Structure and evolution of the western Corinth Rift, through new field data from the Northern Peloponnesus. *Geological Society, London, Special Publications*, 321(1), 119–138. <https://doi.org/10.1144/SP321.6>
- Skourtsos, E., Kranis, H., Zambetakis-Lekkas, A., Gawthorpe, R. L., & Leeder, M. R. (2016). Alpine basement outcrops at northern Peloponnesus: Implications for the early stages in the evolution of the Corinth Rift. *Bulletin of the Geological Society of Greece*, 50(1), 153–163. <https://doi.org/10.12681/bgsg.11714>
- Stefatos, A., Papatheodorou, G., Ferentinos, G., Leeder, M., & Collier, R. (2002). Seismic reflection imaging of active offshore faults in the Gulf of Corinth: Their seismotectonic significance. *Basin Research*, 14(4), 487–502. <https://doi.org/10.1046/j.1365-2117.2002.00176.x>
- Stewart, I. (1996). Holocene uplift and palaeoseismicity on the Eliki fault, Western Gulf of Corinth, Greece. *Annals of Geophysics*, 39(3). <https://doi.org/10.4401/ag-3993>
- Stewart, I., & Vita-Finzi, C. (1996). Coastal uplift on active normal faults: The Eliki Fault, Greece. *Geophysical Research Letters*, 23(14), 1853–1856. <https://doi.org/10.1029/96GL01595>
- Syvitski, J. P., & Milliman, J. D. (2007). Geology, geography, and humans battle for dominance over the delivery of fluvial sediment to the coastal ocean. *The Journal of Geology*, 115(1), 1–19. <https://doi.org/10.1086/509246>
- Turowski, J. M., Rickenmann, D., & Dadson, S. J. (2010). The partitioning of the total sediment load of a river into suspended load and bedload: A review of empirical data. *Sedimentology*, 57(4), 1126–1146. <https://doi.org/10.1111/j.1365-3091.2009.01140.x>
- van Cappelle, M., Ravnås, R., Hampson, G. J., & Johnson, H. D. (2017). Depositional evolution of a progradational to aggradational, mixed-influenced deltaic succession: Jurassic Tofte and Ile formations, southern Halten Terrace, offshore Norway. *Marine and Petroleum Geology*, 80, 1–22. <https://doi.org/10.1016/j.marpetgeo.2016.11.013>
- Watkins, S. E., Whittaker, A. C., Bell, R. E., McNeill, L. C., Gawthorpe, R. L., Brooke, S. A. S., & Nixon, C. W. (2018). Are landscapes buffered to high-frequency climate change? A comparison of sediment fluxes and depositional volumes in the Corinth Rift, central Greece, over the past 130 k.y. *GSA Bulletin*, 131(3–4), 372–388. <https://doi.org/10.1130/B31953.1>
- Whittaker, A. C., Attal, M., & Allen, P. A. (2010). Characterising the origin, nature and fate of sediment exported from catchments perturbed by active tectonics. *Basin Research*, 22(6), 809–828. <https://doi.org/10.1111/j.1365-2117.2009.00447.x>
- Whittaker, A. C., Cowie, P. A., Attal, M., Tucker, G. E., & Roberts, G. P. (2007). Contrasting transient and steady-state rivers crossing active normal faults: New field observations from the Central Apennines, Italy. *Basin Research*, 19(4), 529–556. <https://doi.org/10.1111/j.1365-2117.2007.00337.x>
- Wolman, M. G. (1954). A method of sampling coarse river-bed material. *EOS, Transactions American Geophysical Union*, 35(6), 951–956. <https://doi.org/10.1029/TR035i006p00951>
- Wolman, M. G., & Miller, J. P. (1960). Magnitude and frequency of forces in geomorphic processes. *The Journal of Geology*, 68(1), 54–74. <https://doi.org/10.1086/626637>
- Young, M. J., Gawthorpe, R. L., & Sharp, I. R. (2003). Normal fault growth and early syn-rift sedimentology and sequence stratigraphy: Thal Fault, Suez Rift, Egypt. *Basin Research*, 15(4), 479–502. <https://doi.org/10.1046/j.1365-2117.2003.00216.x>
- Zambetakis-Lekkas, A., & Karotsisis, Z. (1986). Le Jurassique supérieur de la zone de Tripolitza dans la région de Vitina (Péloponnèse Central-Grèce). *Revue De Paleobiologie*, 5, 269–279.

## SUPPORTING INFORMATION

Additional supporting information may be found online in the Supporting Information section.

**How to cite this article:** Watkins SE, Whittaker AC, Bell RE, et al. Straight from the source's mouth: Controls on field-constrained sediment export across the entire active Corinth Rift, central Greece. *Basin Res.* 2020;00:1–26. <https://doi.org/10.1111/bre.12444>